PROCEEDINGS, 44th Workshop on Geothermal Reservoir Engineering
Stanford University, Stanford, California, February 11-13, 2019
SGP-TR-214

Integrating Magnetotellurics, Soil Gas Geochemistry and Structural Analysis to Identify Hidden, High Enthalpy, Extensional Geothermal Systems

Philip E. Wannamaker[1], James E. Faulds[2], B. Mack Kennedy[3], Virginie Maris[1], Drew L. Siler[4], Craig Ulrich[3] and Joseph N. Moore[1]

[1]University of Utah/Energy & Geoscience Institute, 423 Wakara Way, Ste 300, Salt Lake City, UT 84108 USA
[2]University of Nevada, Nevada Bureau of Mines and Geology, 1664 N Virginia St, Reno, NV 89557 USA
[3]Lawrence Berkeley National Laboratory, Center for Isotope Geochemistry, MS 70A-4418, Berkeley, CA 94720-8179 USA
[4]U.S. Geological Survey, 345 Middlefield Road, MS 989, Menlo Park, CA 94025

pewanna@egi.utah.edu

Keywords: Hydrothermal, Hidden Systems, Great Basin, High Enthalpy, Magnetotellurics, Structural Geology, Isotope Geochemistry

ABSTRACT

We applied magnetotellurics (MT), diagnostic structural affiliations, soil gas flux, and fluid geochemistry to assist in identifying hidden, high-enthalpy geothermal systems in extensional regimes of the U.S. Great Basin. We are specifically looking for high-angle, low-resistivity zones and dilatant geologic structures that can carry fluids from magmatic or high-grade metamorphic conditions in the deep crust upward to exploitable depths, and to verify the nature of the deep sources through soil gas and fluid compositions. The project was motivated by prior MT transect coverage of western and central Nevada centered upon the Dixie Valley producing geothermal system where such favorable indicators were first recognized. The high-angle MT structures are taken to be fluidized fault zones connecting deep magmatic/metamorphic activity with the geothermal system, but the concept required verification by testing at other systems.

The project was set up with a two-phased organization. Phase I was carried out at the McGinness Hills system, central Nevada, where Ormat Inc flagship power facility is located and a considerable amount of pre-existing data were available. Transect MT data also showed a strong low-resistivity upwelling originating from interpreted deep crustal magmatic underplating. Controlling structures on production as indicated by Ormat data and our new mapping were favorable to dilatancy, comprising an accommodation zone between major normal faults of opposing dip. A 3D MT survey and inversion confirmed the existence of the steep low-resistivity zone dipping ESE toward the deep crust and placed N-S bounds upon the feature. In cooperation with Ormat personnel, we sampled well fluids from production intervals for He isotope composition. Elevated ^{3}He was verified through mass spectrometry analysis confirming a magmatic connection into the producing system. High CO_2 soil gas flux including possibly metamorphic ^{13}C and ^{14}C component was measured over the area of dilatant structures. Hence, the triad of indicators posed above was confirmed in Phase I.

Subsequently, Phase II of the project proceeded in the greenfield Kumiva-Blackrock Desert district of northwestern Nevada to see if a new system could be identified. Transect MT data also showed a strong low-resistivity upwelling originating from interpreted deep crustal magmatic underplating. An areal MT survey of 131 sites was imaged through 3D inversion using the in-house, DOE-supported finite element algorithm. Particular MT low resistivity upwellings that received followup study occurred under the flanks of the Seven Troughs Range, under Kumiva Playa immediately west of the Blue Wing Mountains, and under northern Granite Springs Valley. Structural assessment of the project area by Co-I J. Faulds at UNR provided numerous favorable Quaternary fault settings, which were correlated to the MT upwelling structures. Soil CO_2 gas flux anomalies generally were not large but did show correlation with MT upwelling structure and favorable geological structures. Isotope analyses showed presence of possible inorganic/metamorphic ^{13}C but ^{14}C concentrations did not exceed background values.

We view the initial concept of a confluence of MT low-resistivity upwelling, favorably dilatant 3D geological structure, and elevated soil gas flux including ^{13}C component to be supported by the further evidence of this project although the indicators in the Phase II study were more diffuse. Mass balance calculations based upon ^{3}He R/Ra values indicates that the proportion of magmatic fluids in a producing system is fairly low, 10-15% by volume. We suggest that the diagnostic MT geophysical structures denote zones of concentrated extensional deformation that increases permeability, potentially enabling a circulating upper crustal geothermal system, while at the same time connecting telltale deep component signatures to the upper crust. The northern Granite Springs Valley structure is receiving followup study and drilling in the University of Nevada Reno Play Fairway Analysis, being at the southern termination of a major normal fault with silicified soil and slightly elevated temperature probe results.

1. INTRODUCTION

This project has been combining 3D magnetotellurics (MT), soil gas flux and geochemistry and structural geology into a multi-method, integrative technology for identifying blind, high temperature, high enthalpy geothermal resources. Reconnaissance MT surveys show that the onset of low resistivity in the deep crust generated by active magmatic underplating and fluid release may come to remarkably shallow depths in areas of high rates of recent extension (Wannamaker et al., 2006, 2011; Siler et al., 2014; Dobson, 2016). Commonly, steep crustal-scale fault zones connect this deep conductor to high temperature geothermal systems near the surface (Wannamaker et al., 2011; Siler and Kennedy, 2016). As structural analyses have accumulated, systems are increasingly recognized to form in zones of structural complexity and dilatancy of various possible types, including horsetailing fault terminations, step overs (or relay ramps), and

accommodation zones (Faulds and Hinz, 2015). Moreover, high-T geothermal systems sometimes show gas or fluid compositions with deep crustal and/or mantle fluid contributions. However, as we discuss further, prior to this project Dixie Valley appeared to be the only Great Basin extensional system where all three methods converge to present a unified picture. We have aimed to show this is no accident by applying the methods to a newly exploited geothermal system in Phase I (McGinness Hills), and in Phase II utilizing these methods to identify heretofore unrecognized blind geothermal systems (Black Rock-Kumiva Desert region).

We performed proof-of-concept in the Phase I study using the hitherto blind McGinness Hills system of central Nevada as a natural laboratory (Nordquist and Delwiche, 2013). Reconnaissance MT profiling (2D) had revealed that McGinness Hills also has a strong deep crustal source and a steep fluidized fault zone feeder. To confirm the 2D MT structure, we planned to carry out detailed 3D MT surveying to delineate the volumetric topology of low-resistivity upwellings, soil gas flux surveying (primarily CO2) along with fluid and isotope geochemistry to confirm that the upwellings are carriers of deep-crustal, high-T fluids, and thirdly structural analysis to evaluate whether diagnostic structures can be identified which control the fluid upwellings. If these indicators all turned out positively at McGinness Hills, it would confirm this reconnaissance exploration paradigm and motivate moving to a greenfield area in Phase II to seek new, hidden potential geothermal systems. A larger investigation of the Black Rock-Kumiva Valley area of northwestern Nevada would be this greenfield area as it shows pronounced upwelling of deep crustal low resistivity in the prior Great Basin transect MT surveying and lies in a zone of active, ongoing extension that contains several favorable structural settings for geothermal activity.

2. TECHNICAL APPROACH AND OBJECTIVES

Our concept is represented in Figure 1 which combines 2D transect and dense profiling MT models centered over the Dixie Valley producing field, west-central Nevada. A steep crustal conductor interpreted as a major fault zone, confirmed in subsequent 3D MT surveying (Wannamaker et al., 2013), carries magmatic fluids from probable deep crustal igneous underplating to the west (Buena Vista-Humboldt zone) into the Dixie Valley geothermal system. It is interpreted as underplating because of likely temperatures and oxidation state, and because existing seismic studies (COCORP, PASSCAL) resolved V_P attenuation, high V_P underplate and high reflectivity there (Catchings and Mooney, 1991; Wannamaker et al., 2007; 2008). Mantle sourced ^{3}He anomalies corroborate this (Kennedy and van Soest, 2007; Siler and Kennedy, 2016), and the situation fits into the general deep hydrological/magmatic paradigm of Crossey and Karlstrom (2012) (Figure 1). An important factor in bringing exploitable fluids surfaceward at Dixie Valley is the intersection of N-S and NE-SW fault trends (Faulds et al., 2011), also resolved in 3D MT surveying (Wannamaker et al., 2013). However, prior to this project, Dixie Valley was the only system known in the Great Basin where such crustal resistivity structure, isotope geochemistry and permissible structures coincided. To validate that MT is reliably imaging magmatic source connections to the near-surface, we initially aimed to demonstrate the confluence of these three lines of evidence at another geothermal system.

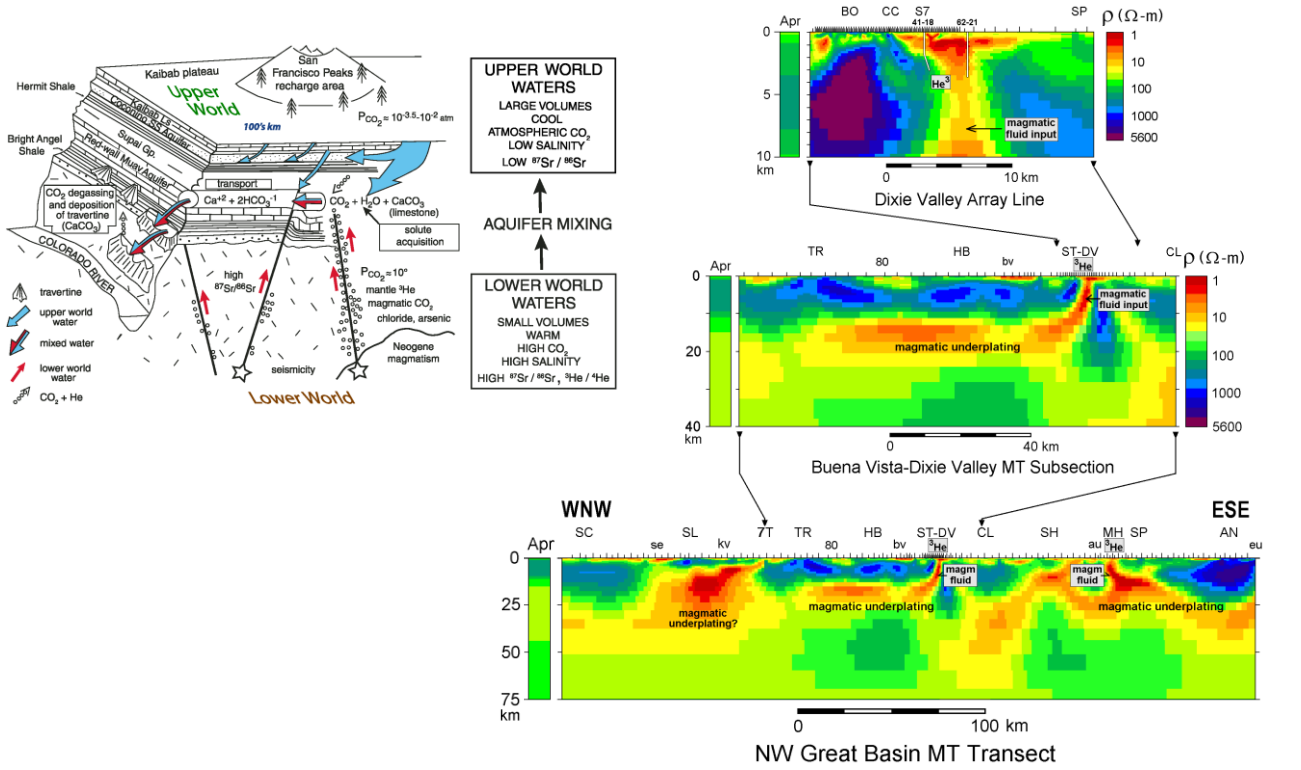

Figure 1: Right: 2D MT resistivity inversion section views centered upon Dixie Valley, Nevada (Wannamaker et al., 2007, 2011; Siler et al., 2014; Dobson, 2016). Upper panel includes dense array data to provide a detailed system view through the producing area and Cottonwood Canyon. Left: Conceptual model of Crossey and Karlstrom (2012) of crustal-scale hydrology including magmatic input based upon regional travertine occurrences and spring chemistries.

In addition to Dixie Valley, two other prominent zones of conductive upwellings are observed in Figure 1, the recently recognized McGinness Hills area east of Austin (au) and the San Emidio-Kumiva Valley (se-kv) area southeast of the town of Gerlach. All these zones were highly resolved in the data, demonstrating pronounced vertical current gathering effects (Wannamaker et al., 2006a,b). We selected McGinness Hills as a natural laboratory under Phase I because it was newly under development, there were geothermal wells which could be tested for magmatic components (particularly ^{3}He anomalies) for consistency with surface indications, and the operator Ormat Inc had substantial in-field information. A well-resolved, fully 3D resistivity picture established with a new MT survey was considered probable as overburden thicknesses were limited and topography was modest. Favorable geological structures associated with geochemical anomalies were to be sought that could confirm upwelling of fluids suggested by the geophysics. Thus, an overall project goal as been to test whether MT geophysics can take a leading role in the mid-scale assessment of new geothermal resource areas and hence provide targets for detailed followup incorporating additional techniques (structural and soil gas analyses).

If McGinness Hills with its available in-field data supports the magmatic concept we consider, the methodology would be tested in the Phase II application in the more greenfield San Emidio-Black Rock Desert-Kumiva Valley region of northwestern Nevada. This is a larger region with no deep wells to sample other than those of the San Emidio geothermal field on the western margin of the project area. However, as inversion of newer, larger-scale transect MT data shows (Wannamaker et al., 2011; Siler et al., 2014), the Black Rock-Kumiva Valley area possesses the largest, most pronounced conductive upwelling across the entire Great Basin at this latitude (Figure 1). Examination by Faulds and coworkers (Forson, 2014; Forson et al., 2014) suggests several promising structural settings in this actively extending region. Crustal-scale plumbing has existed in this region for an extended period of time, as several Pliocene epithermal mineral deposits are spatially associated with currently active geothermal systems (e.g., San Emidio-Wind Mountain, Florida Canyon-Humboldt House, and Hycroft-Lewis) (Coolbaugh et al., 2005; Faulds et al., 2005; Rhodes et al., 2010; Rhodes, 2011). A success in Phase II would complete a foundation for the MT method serving as a mid-scale reconnaissance tool in locating potential high-T, blind fluid upwellings suitable for multi-technique followup to vector into potential hidden geothermal systems.

3. MCGINNESS HILLS SYSTEM INVESTIGATION

When the low resistivity crustal upwelling of Figure 1 was first identified in 2006, McGinness Hills geothermal development was just beginning (Nordquist and Delwiche, 2013). The low-resistivity had a strong influence on the MT transect data in this area but full geothermal significance was not yet recognized. A primary purpose of this followup study is to assess reliability of the resistivity using 3D coverage and inversion, clarify existence of controlling dilatant structures, and test deep crustal communication using isotope geochemistry.

3.1 Magnetotelluric (MT) Survey and Inversion

Seventy (70) new MT stations under subcontract were added in the summer of 2012 to those of our legacy transect of Figure 1. Ormat Inc. donated the responses from their own dense array surveying prior to drilling from which several individual sites were selected to gain a total of 96 sites (Figure 2a). The 70 new sites were permitted with the Bureau of Land Management (Battle Mtn Office, 54 sites) and the U.S. Forest Service (Ely Office, 16 sites).

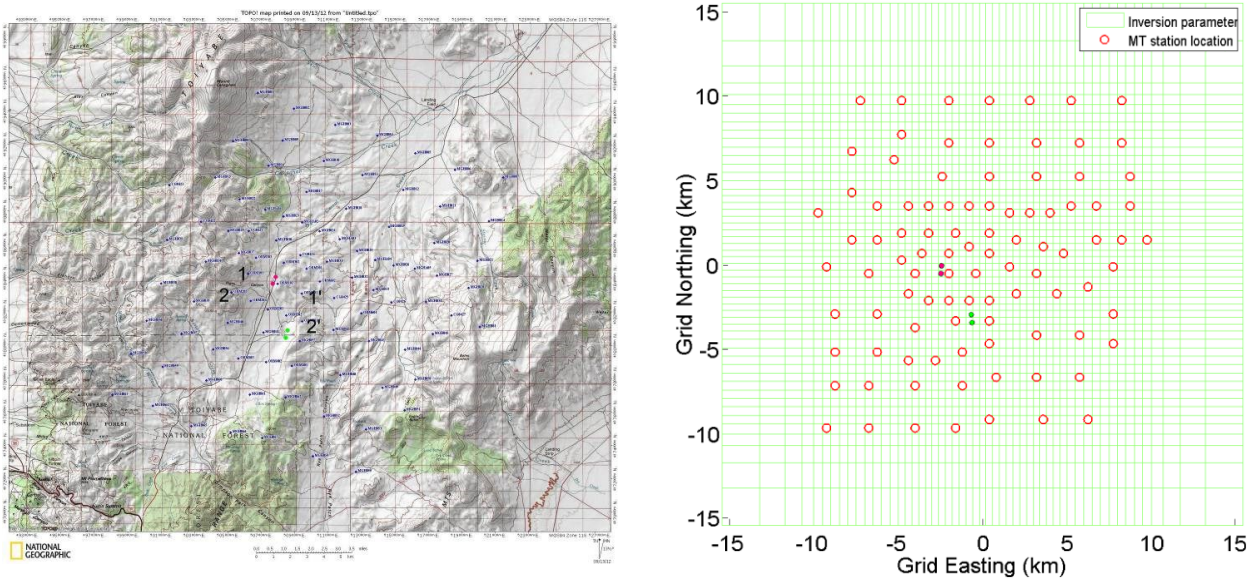

Figure 2. Left: Distribution of 96 tensor MT soundings of the McGinness Hills geothermal area, central Nevada. Pairs of red and green dots denote locations of production and injection well pads. Right: Parameter grid and station locations for 3D MT resistivity inversion. Inversion grid northing is rotated 20 deg CW wrt geographic north. Points 1-1' and 2-2' denote endpoints of dense MT array profiles of Ormat whose inversion models appear in Figure 3.

Two detailed though shallow inversion images from the Ormat dense array MT data as produced by their contractor appear in Figure 3. Line 1 runs essentially through the production wellpad while Line 2 runs parallel but ~1 km to the south (Figure 2). In the line 1 image,

we denote two subvertical conductors A and B. Conductor A corresponds positionally to the projection of the crustal-scale steep conductor of the original transect inversion (Figure 1). Branching to the west is B, which appears to be the feature tapped by the producing wells (B. Delwiche, pers. comm.). This demonstrates the need for detailed followup of initial structural imaging to identify fine scale structure pertinent to the shallow targets of the current development. However, at least as important as the resistivity structure in defining drilling targets were the results of shallow slimhole drilling and structural geology mapping (Nordquist and Delwiche, 2013; B. Delwiche, pers. comm.).

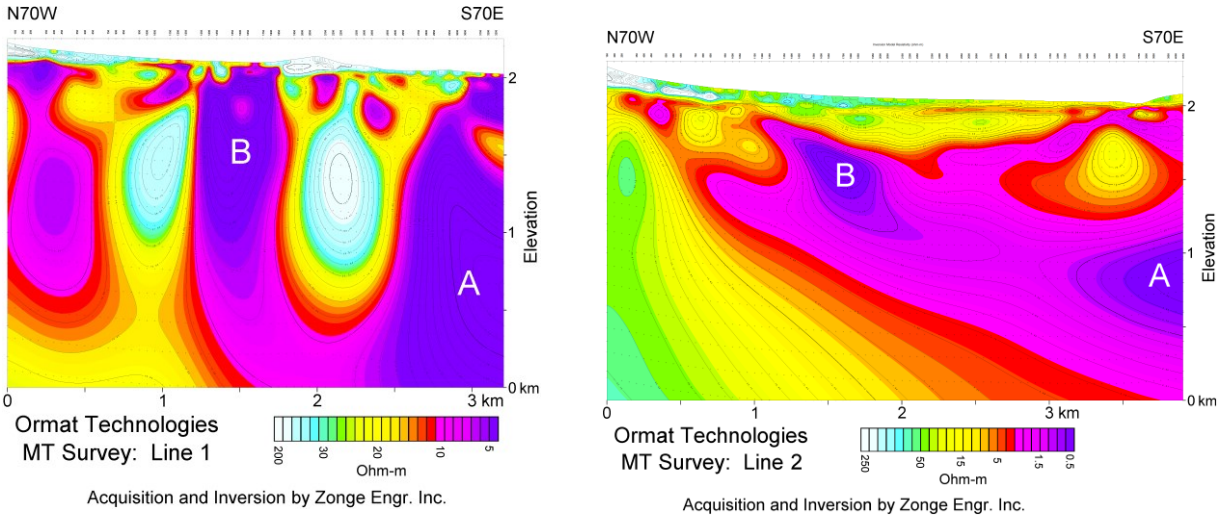

Figure 3. Smooth structural inversions of array MT data acquired by Zonge Engineering Org for Ormat Technologies across the central McGinness geothermal field. Location of profiles in left side of Figure 2.

The 96 distributed MT soundings underwent 3D inversion using the U Utah software based on the code of Sasaki (2004) parallelized as in Maris and Wannamaker (2010). This is a Gauss-Newton algorithm that seeks to fit the measured responses using a model smoothed spatially in the x-y-z directions (Tarantola, 1987). The finite difference simulation mesh had dimensions 98x 103y 59z which in turn were grouped to give 95x 100y 43z inversion parameters (Figure 2b). The modest degree of topography was not considered (flat earth model). The top voxel was 60 m thick, and the total mesh depth was 19 km. With error floors of 5%|Zxy-Zyx|/2 on impedance elements and 0.05 on tipper elements, starting nRMS was 19.3 ending at 1.71. This is a good fit giving a well resolved resistivity model (Figure 4). We have examined ~20 levels of the 3D structure in detail and present four especially pertinent slices in Figures 4a and b. One of the levels shown is near 1 km depth, close to the main producing intervals, and the other toward 3 km depth which is near the top of the deep crustal upwelling seen in the original transect study.

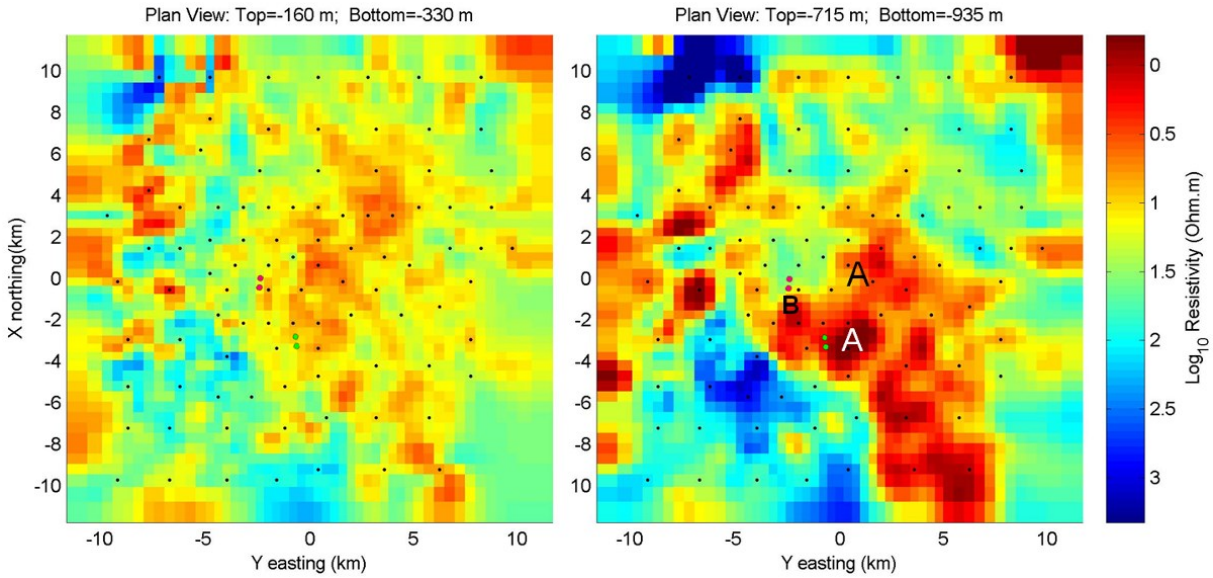

Figure 4a. Two representative plan views at shallow depths through 3D resistivity model of McGinness Hills MT survey. Conductors B and A denote areas of production and the crustal-scale magmatically connected structures respectively.

The shallowest model level in Figure 4a (160 – 330 m) shows a quasi-continuous low-resistivity layer over the survey that likely represents old alteration from the Oligocene blanket of tuff overlying much of the area, as will be shown more clearly in the upcoming structural sections. However, the next level (715 – 935 m) shows structures most likely below the tuffs. We have labeled particular features A and B, which correspond to the conductors noted in the dense array sections of Figure 3, the latter of which represents the production zone and the former being the 3D representation of the top tip of the regional conductor of Figure 1. Conductor B may merge at depth with the larger-scale crustal conductor A which suggests that a large, deeper resource could be present nearby to the east. We are struck by the pronounced SE grain to the larger-scale conductor A at its deeper levels (2675 m and beyond). As discussed with the new structural geology work below, we interpret this to reflect control by pre-Basin and Range structural trends which have become dilatant under east-west directed extension.

At greater depths (Figure 4b), the multiple conductors merge and continue to dip in a southeasterly direction toward the deep crust compatible with the regional structure in Figure 1. The panels in Figure 4b show the 3D expression of the steep 2D transect conductor and are well resolved as they are responsible for replicating the strong vertical current channeling effects visible in the original transect pseudosections (Wannamaker et al., 2006a,b). These effects are visible in the areal sounding coverage along the strike length of the A conductor. The 3D image now resolves the finite strike of this crustal break and the geometric orientation of its grain.

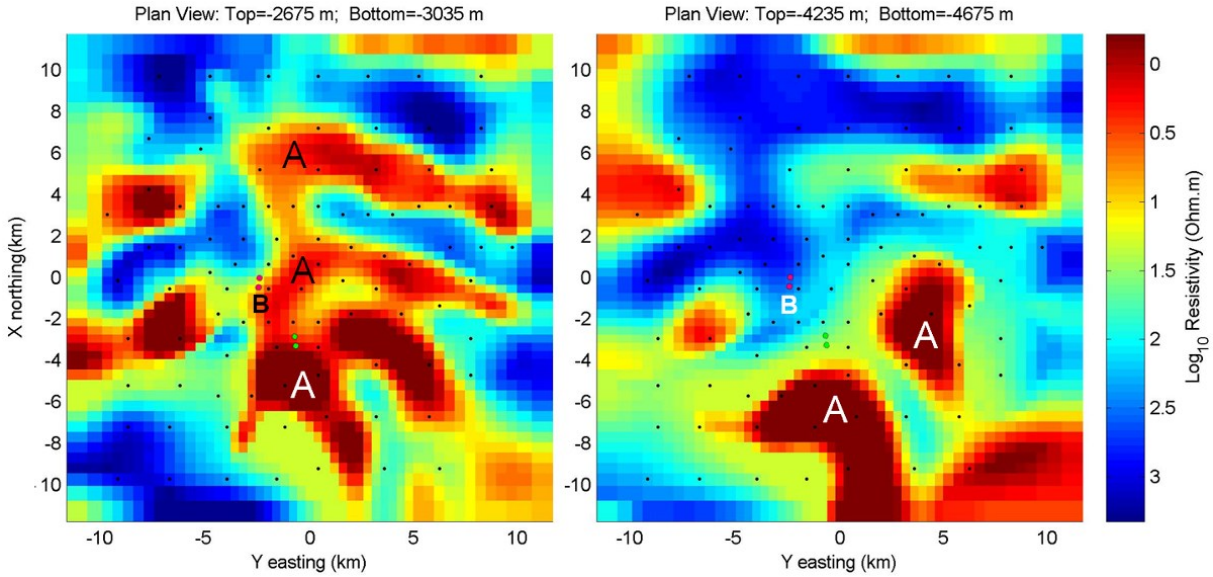

Figure 4b. Two representative plan views at greater depths through 3D resistivity model of McGinness Hills MT survey. Conductors B and A denote areas of production and the crustal-scale magmatically connected structures respectively.

3.2 Geological Mapping and Analysis

Coauthors Siler and Faulds undertook 20 days of new geologic mapping of over 60 km^2. They held detailed meetings with structural geologist B. Delwiche of Ormat at the latter's sample facility in Reno and examined the mud logs and downhole data to obtain subsurface constraints for the 3D structural model. The McGinness area is dominated by gently east-tilted fault blocks bound primarily by moderately to steeply west-dipping normal faults (Figure 5). Fault blocks consist of Oligocene-early Miocene ash-flow tuffs overlain by andesite lavas that nonconformably overlie Paleozoic metasedimentary rocks locally intruded by Jurassic plutons. Quaternary alluvial fan deposits onlap all older rock units. The geothermal system lies in a hybrid structural setting (Faulds et al., 2013; Faulds and Hinz, 2015). On a regional scale, the structural setting is characterized by a broad accommodation zone, which includes the west-dipping range-front fault of the Simpson Park Range (SPF) and a major east-dipping fault on the east side of the Toiyabe Range (ETRF) (Figure 5 left, inset). The geothermal system essentially occupies an interbasinal high between the Big Smoky and Grass Valley basins at the confluence of the Toiyabe and Simpson Park Ranges.

On a local scale, however, the McGinness Hills system occupies a left step-over within a north-northeast-striking, west-dipping normal fault system in a belt of overlapping east- and west-dipping faults (Figure 5, Faulds et al., 2013). Highest permeability appears to reside at the intersections of the NNE-striking faults with NW-striking, steeply dipping faults. Some of the NW-SE oriented faults may be reactivated, pre-Basin and Range trends possibly as old as Oligocene as such faults locally appear to have controlled the thicknesses of silicic tuffs of that age and juxtaposition of old and new sustems (Casaceli et al., 1986; B. Delwiche, pers. comm..). They roughly parallel the trends resolved in the deeper MT resistivity image associated with conductor A. It is no surprise in geothermal systems that intersecting fault trends with different ages of origin may control permeability of the system (e.g., Faulds and Hinz, 2015). Nevertheless, the existence of a faulting framework over a protracted depth range which can generate dilatancy supports our principal hypothesis that upwelling low resistivity originating from substantial depth in the active Great Basin represents deep-seated fluid flow with possible magmatic roots that is reaching exploitable resources. The remaining task is to see if geochemical indicators either from soil gas or well fluids further corroborate this concept.

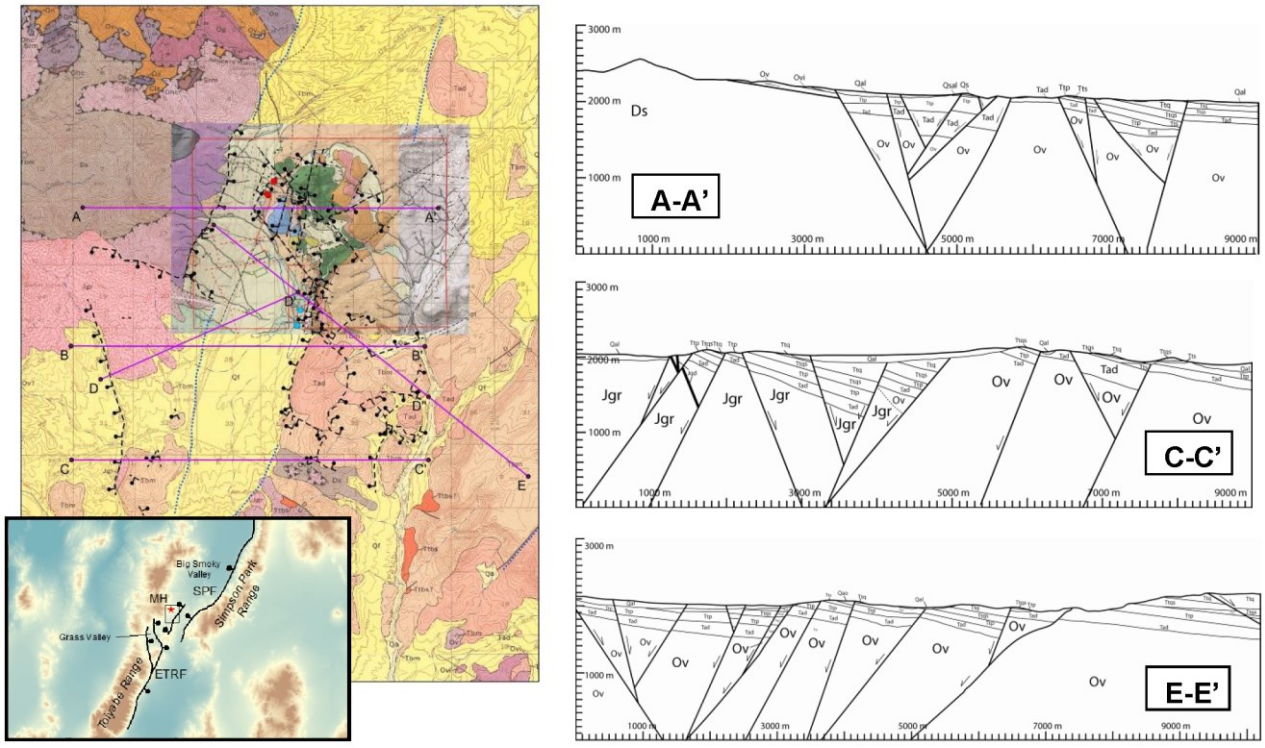

Figure 5: New fault mapping are and detailed cross sections through the producing and injecting areas in the McGinness Hills by coauthors Siler and Faulds incorporating Ormat in-field data in cooperation with B. Delwiche. Lower inset shows production area (red box) inside larger structural accommodation zone (black border). Relation of larger-scale faults entering the field from north and south are displayed and discussed more by Faulds et al. (2013).

3.3 Production Fluids and Soil Gas Geochemistry

With kind assistance of Ormat personnel, four ^{3}He samples were taken from production wells at McGinness Hills (Figure 6). Two were from the easterly 36-10 well pad from depths of ~2100 ft (640 m) and two from the westerly 28-10 pad from depths of ~3200 ft (975 m). These intervals both are from west-dipping fault zones. Tracer and pump tests indicate that all production and injection intervals appear to be in strong inter-communication (B. Delwiche, pers. comm.). The four ^{3}He samples were analyzed at the Center for Isotope Geochemistry at LBNL and found to be generally clean of atmospheric contamination. R/Ra values ranged from 0.35-0.49 in 36-10 fluids to 0.41-0.57 in 28-10 fluids. While these do not rival the high magmatic values seen at Coso or some Cascades volcanoes, they are significantly above the Great Basin background value of ~0.1 (Kennedy and van Soest, 2006, 2007; Siler and Kennedy, 2016), signifying that, like the Dixie Valley system, deep seated fluids are entering the McGinness Hills hydrothermal system. The R/Ra values appear to increase with depth in the reservoir, consistent with upwelling of deeper fluids carrying a mantle signature. Thus the helium isotopic data support our hypothesis that the MT low resistivity structure connecting to the lower crust is tied to deep magmatism (e.g. crustal underplating) and represents a crustal-scale pathway experiencing fluid flow. The helium isotopic compositions (0.35-0.57 Ra) indicate that ~5-10% of the McGinness Hills helium is mantle derived (Kennedy and van Soest, 2006, 2007). However, this amount may differ from the long term average depending upon deformation and seismicity, as exemplified in the Mammoth Hot Springs district (Sorey et al., 1998). At the very least, it reflects the fact that special extensional conditions were created through this crustal column sufficient to allow large-scale if episodic permeability. It may point to an ultimately larger exploitable reservoir in the long run.

A total of eight soil gas flux transects were completed over the McGinness Hills area (Figure 7a). The single transect line (B, Figure 7a) was conducted in the vicinity of the injection wells south of the producing field. The E-W transect crossed a N-S trending fault believed to mark the eastern boundary of the reservoir system. No soil flux anomalies were observed. The remainder of the transects (A, Figure 7a) focused on the fault accommodation zone that hosts production. A detailed map of the transects and their relationships to the faults mapped is given in Figure 7b. In general, the observed CO_2 fluxes are low when compared to those associated with active crustal volcanic systems or surface manifestations of deep hydrothermal systems (e.g. fumaroles, hot springs, etc.). The low values have made interpretation difficult. However, it is clear that for the most part only a few significant anomalies were observed. They are in portions of the transect lines MG913-E, MG13-A, MG13-B and MG12-A. MG913-E was acquired one week after the McGinness Hills area experienced significant rainfall. It is likely that the consistently elevated fluxes along that entire transect reflect renewed plant activity resulting in high root CO_2 respiration.

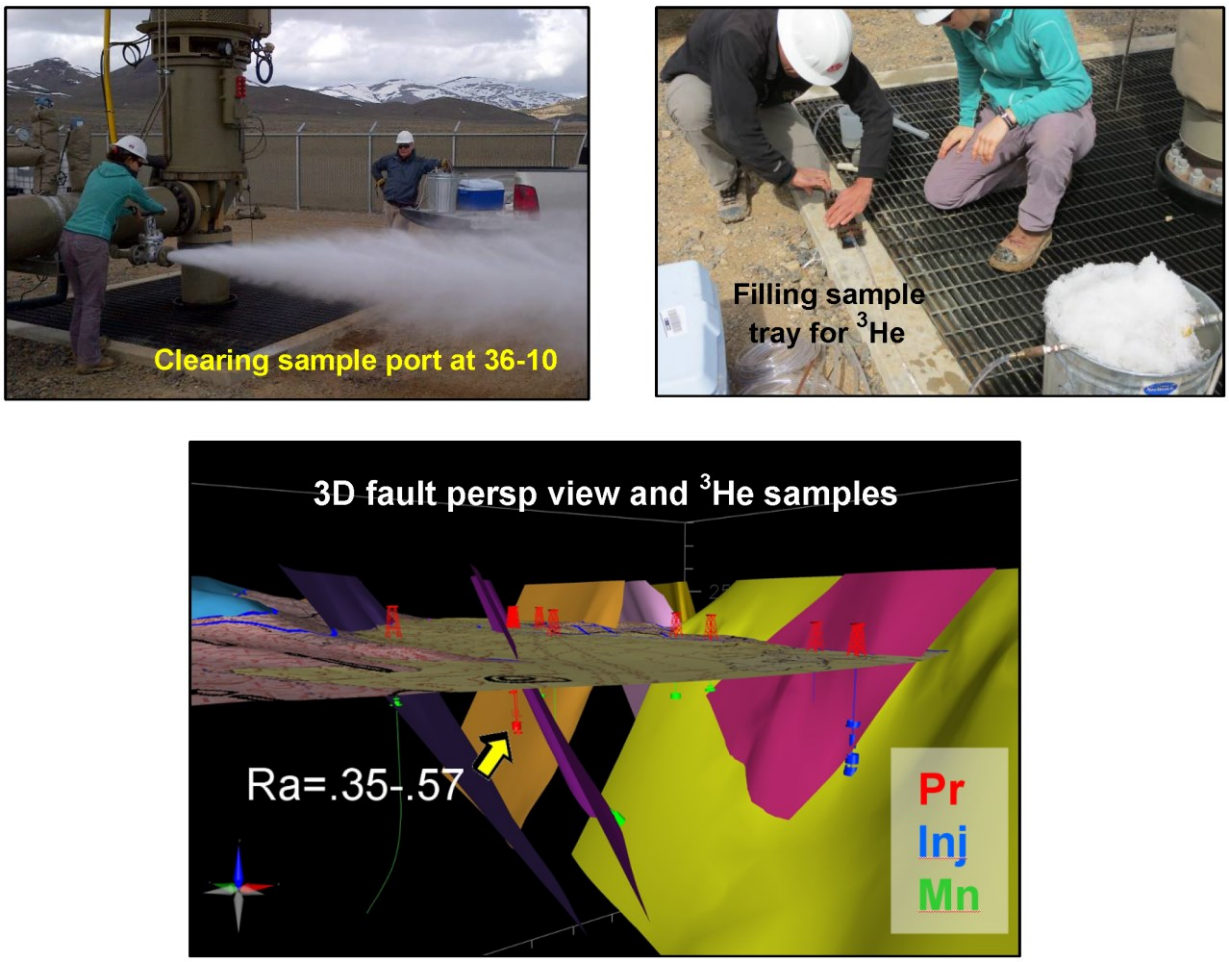

Figure 6: Procedures and results of sampling for ^{3}He at McGinness Hills. Production zone fluids were sampled and analysed using trays supplied by LBNL (upper right) (L. Owens, B. Delwiche). R/Ra label points to sample production interval of 28-10. Photos by Phil Wannamaker, with permission. Structural rendition supplied by B. Delwiche, Ormat.

The remaining transects were acquired in late August, 2012 and 2013, during the peak of the dry season. We identified three areas of interest where repeated measurements consistently indicated elevated CO_2 flux with respect to the surrounding areas. These areas are indicated by the white circles in Figure 7b. It is noteworthy that all three of these high flux areas are within a set of N-S striking normal faults (pink and blue, Figure 7b), particularly where these faults encounter the extensive NW-SE reservoir bounding fault (orange line), almost directly south of the silica sinter mound in the eastern part of section 10 (Figure 7b). Consistently, the high values are seen immediately west of the N-S striking faults. It is not necessary that high flux values be associated exactly with a fault surface trace; even if carried in a fault zone, gas may exit to the surface before that trace is reached. In a lithologic column of quartzites and granitic intrusions, a high CO_2 flux is consistent with a deep high-T source. We did not observe enhanced CO_2 flux farther east (transect MG13-C) toward where the large crustal conductor B would project surfaceward. It may be that the altered tuff blanket is preventing vertical gas movement to shallow soil levels. However, the fact that ^{3}He was observed in connection with produced fluids is still confirmatory.

To help determine the source of the elevated CO_2 gas fluxes in the identified areas of interest, indicted by the white ellipses (Figure 7b), a suite of soil gas samples was collected at ~0.5-1.0 meter depths using a pipette probe and analyzed for CO_2 concentration and carbon isotopic composition (Figure 8). The observed co-variation between del^{13}C and inverse CO_2 concentrations indicates that the soil gas samples represent mixtures of two CO_2 sources. The inferred composition of the first source (A, Figure 8) is consistent with the composition of CO_2 respired from plant roots (del^{13}C ~ -18 to -22 per mil) (Cerling et al., 1991; Amundson et al., 1998). The two soil gas samples most enriched in this component (transect MG13-A, del^{13}C ~ -18 per mil; transect MG13-B, del^{13}C ~-14 per mil) were located in low lying areas related to a NW-SE trending drainage system, characterized by more extensive vegetation. The second CO_2 source (B, Figure 8) appears to have a carbon isotopic composition similar to atmospheric CO_2 (del^{13}C > ~ -7 per mill). However, the CO_2 concentration must be significantly less than the present day atmosphere (~400 ppmv). The samples most enriched in component B (del^{13}C > -14 per mil) are from within the white circle along transect MG12-A. They were collected along an upslope with sparse vegetation terminating in a saddle-like structure at the intersection of the blue and orange faults.

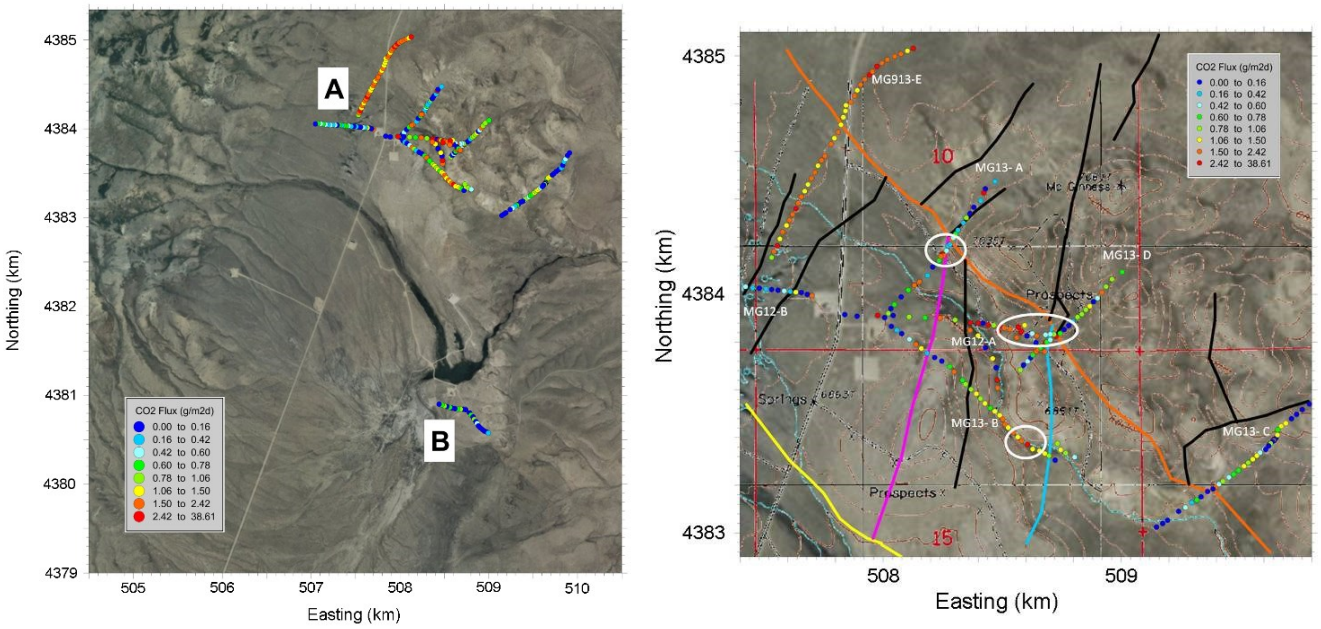

Figure 7: (a, left) Overview of results of the CO_2 flux surveying surveying at McGinness Hills. (b, right) Detailed map of survey locations within the accommodation zone. Each dot in shows a GPS-referenced flux sample location. Warm colors correspond to high gas flux values. Black, orange, yellow, blue and pink lines correspond to faults. White ellipses indicate areas of interest with relatively high CO_2 fluxes. These areas were selected for soil gas sample collection for carbon isotope analyses.

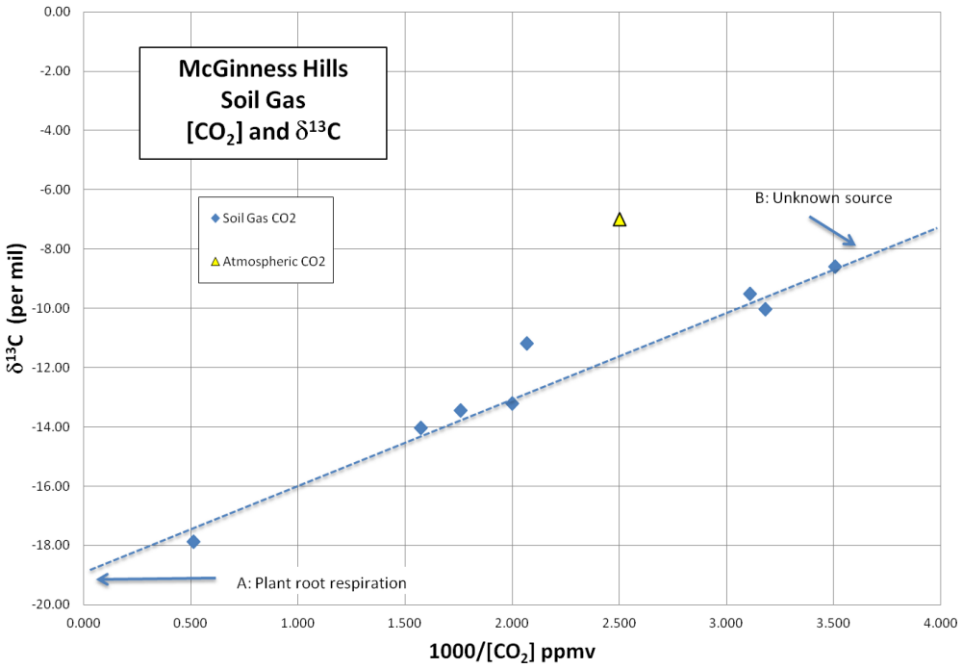

Figure 8: CO_2 concentrations and carbon isotopic of soil gas samples collected from the areas of interest (AOIs, white circles in Figure 7b).

The origin of component B is not presently constrained by the ^{13}C data. However, the isotopic composition is consistent with a deep abiotic (hydrothermal) source but the low CO_2 concentration is puzzling, requiring that either CO_2 is being lost from the system by geochemical processes (precipitation of calcite, adsorption on clays, etc.) or the depleted concentration reflects a sampling artifact. To better constrain the source, soil gas samples were sent to the Center for Accelerator Mass Spectrometry at Lawrence Livermore National Lab for ^{14}C analyses. If the samples consistently contain 100% modern concentrations of ^{14}C, then the unknown CO_2 source must be related to the atmosphere and/or plant production. If, on the other hand, the samples are depleted in ^{14}C relative to modern day carbon, then the source must have a deeper abiotic origin.

The ^{14}C results ranged from ~87-102% modern carbon (+/- 0.3-0.7%, 1 sigma). A one-to-one correlation between ^{13}C and percent modern carbon was not observed (Figure 9). However, two samples enriched in heavy carbon (del^{13}C > -12.0) were found to be depleted in ^{14}C relative to modern air, although the depletions are small (~87-92% modern). It is likely that these samples are indicative of CO_2 input from deeper sources. Yet it is clear, the CO_2 soil gas system is complex with at least three independent CO_2 sources: root respiration, air, and deeper abiotic CO_2.

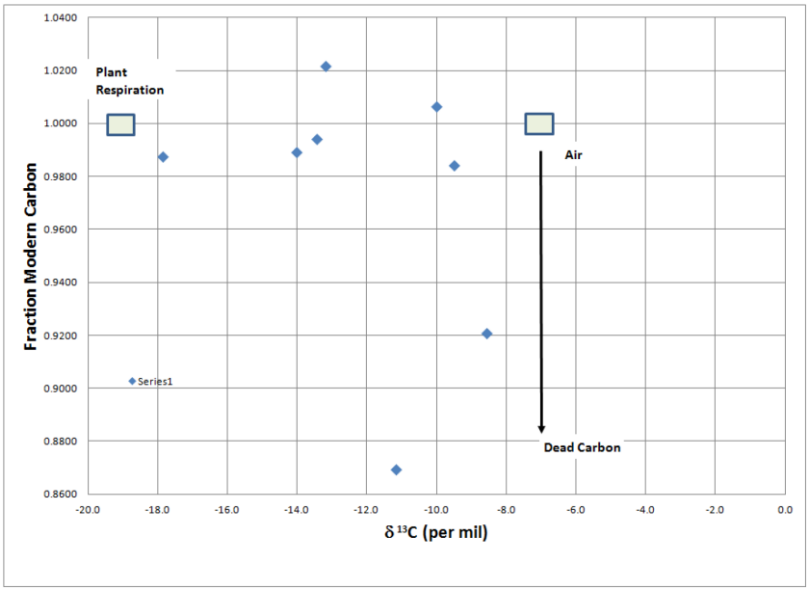

Figure 9: Comparison of the fraction of modern ^{14}C and ^{13}C for McGinness Hills soil gas samples.

3.4 Age dating of siliceous sinter

No hotsprings or other modern thermal features mark McGinness Hills, making it technically a blind geothermal system, although high temperatures in wells drilled to ~1000 feet depth for gold exploration and high fluid geochemical temperatures from sampled well fluids were encountered (Nordquist and Delwiche, 2013). However, hydrothermal opal and chalcedony exists ~1 km southeast of the producing wells in a prominent mound and as alluvial cement. Dating of adularia in quartz veins within the silica mound by the K-Ar method yielded ages of 2.2 and 3.2 m.y. (+/- 0.4 Ma) (Casaceli, 1986).

As an independent assessment of silica mound and geothermal system age, four separated samples of siliceous sinter were acquired, three as massive sinter from the mound and one from extensively silicified alluvium (Figure 10). These were delivered to the Rafter Radiocarbon laboratory of GNS Science, Lower Hutt, New Zealand, for accelerator mass spectrometry (AMS) analysis. Samples were pretreated via H_2O_2 soaking, then crushed, with carbonates and silica dissolved via acid. Specific plant material sought for dating was pollen, under the assumption that this would be trapped at time of silica formation and did not infiltrate the silica later. Carbon dioxide was obtained by sealed-tube combustion, and converted to graphite by hydrogen reduction over iron catalyst.

As labeled in Figure 10, the calculated ages are all quite young (7425 – 14994 a). Computed error on sample SI-1 was 257 a and the errors on the remaining samples were all <100 a. This is remarkably younger than the reported K-AR dates above. A concerted effort was made to avoid sample contamination in the ^{14}C dating by targeting the pollen, although it is difficult to guarantee against truly unknown factors. Erroneously high K-Ar computed ages may occur through introduction of excess ^{40}Ar, perhaps by entrainment of older mineral material such as from a suspected Oligocene porphyry intrusive below McGinness Hills (Casaceli, 1986). We note that sample SI-2 resided at a lower elevation than older sample SI-1 (Figure 10), presumably reflecting the common occurrence of earlier silicification presenting a vertical barrier to later emplacement (Casaceli, 1986).

3.5 Conclusions of McGinness Hills Study

The goal of the Phase I effort was to show that a positive intersection of our three principal techniques can confirm the existence of high-temperature source regions below a geothermal system. Specifically what we mean here vis-à-vis the goal is that a second geothermal area, in this case advantageously including well control (McGinness Hills), can be shown to possess MT structure reflecting magmatic intrusion deep in the crust and a fluidized damage zone to higher levels connecting with the geothermal system. The independent confirmation has been met with the McGinness Hills study, a geothermal system where a deep-seated, magmatically related MT structure was implied prior to system confirmation. A fully 3D MT survey has established that the original reconnaissance resistivity structure is no 2D artifact, but 3D coverage certainly is worthwhile to establish system bounds and structural character. New structural mapping and modeling has demonstrated existence of favorable NW-SE oblique structures and fault structures in a broad accommodation zone. According to the 3D MT, this structural trend appears to continue to depth and iinfluences the deep upwelling.

The CO_2 flux surveying to date shows enhanced flow at or near fault intersections and some major faults within the accommodation zone. Elevated CO_2 flux is associated with enriched ^{13}C content, which is suggestive of deep crustal input given the siliciclastic and intrusive host compositions. The ^{14}C analyses appear to confirm some deep crustal source input, though not large. More importantly, the helium isotopic compositions in the production well fluids show elevated ^{3}He R/Ra values, indicating an influence on the geothermal system from the deep-seated, magmatically related structure seen with MT. The apparent volume of magmatic fluids is only ~10% at such R/Ra (see Kennedy and van Soest, 2006). We suggest that the locally vigorous, crustal scale extension that enables deep magmatic emplacement and leakage into the system also enables upper crustal meteoric fluid convection that establishes the producing geothermal reservoir. The favorable coincidence of geological and MT structures with magmatic geochemistry seen earlier at Dixie Valley was no accident. The positive results from McGinness Hills warranted the decision to proceed to Phase II research to explore the concept in a truly greenfield area without well control, in this case the Kumiva-Black Rock area.

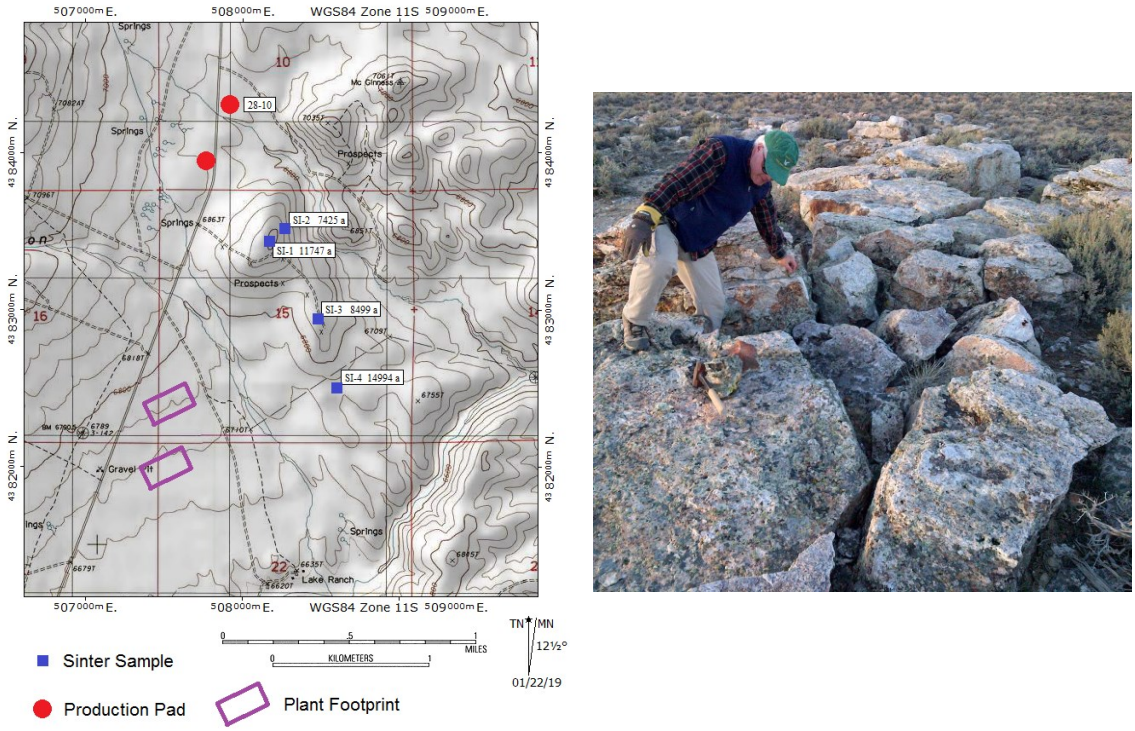

Figure 10: Left (a), topographic image showing locations of four siliceous sinter samples (SI-#) near the McGinness Hills geothermal system. Ages in years are listed in text boxes. Production well pads are as of 2014, and well 28-10 where anomalous ^{3}He R/Ra values were recovered (Figure 6) is labeled. Right (b), Well-exposed siliceous sinter near top of main mound ~0.75 km southeast of production pads. Photo by Ben Delwiche..

4. KUMIVA DESERT SYSTEM INVESTIGATION

The plan for the BlackRock-Kumiva district in Phase II involved an initial, broad-scale structural reconnaissance based mainly upon existing imagery and initial field trips to guide placement of the 3D MT survey so that obvious favorable structural settings receive good spatial sampling. However, the primary criterion for the MT layout is to cover in fully 3D fashion the anomalous structure imaged in the original 2D transect data of Figure 1. This is a larger area than that at McGinness Hills and requires more sites for coverage. Nevertheless, the station spacing would be somewhat greater and this constitutes a test of the scale of a greenfield area that our approach may be able to address.

Subsequently, any prominent localized, shallowing low-resistivity imaged by the 3D MT inversion would receive structural analysis to determine if a favorable setting exists from surface indications of potential structural complexity and dilatancy that can permit deep fluid upwelling. Presuming that surface fault structures are resolvable, soil gas geochemistry was to be surveyed in detailed transects to search for indications of deep abiotic gas components. The goal of Phase II is to provide a third example confirming that shallow crustal MT extensions from deep crustal high-T zones reflect upwelling fluids. It is to be an example established without information from existing geothermal resource development such as at McGinness Hills.

4.1 Magnetotelluric (MT) Survey and Inversion

Under the MT project component, 110 new soundings were gathered over the Seven Troughs-Kumiva Valley-Selenite Range area, adding to 21 prior transect sites for a total of 131 sites to be analyzed (Figure 11a). Surveying extended just westward enough to cover the San Emidio producing geothermal system. Data acquisition was contracted to Quantec Geoscience Inc., the same consultancy that

acquired the prior transect MT data and the data at McGinness Hills. Because the GWe-scale Bonneville Power Authority DC transmission line runs past the San Emidio system, an ultra-remote reference site was installed ~200 km away east of the village of Midas, NV (Figure 11b), for DC line noise suppression, a known hazard for MT surveying in this region (Wannamaker et al., 2004).

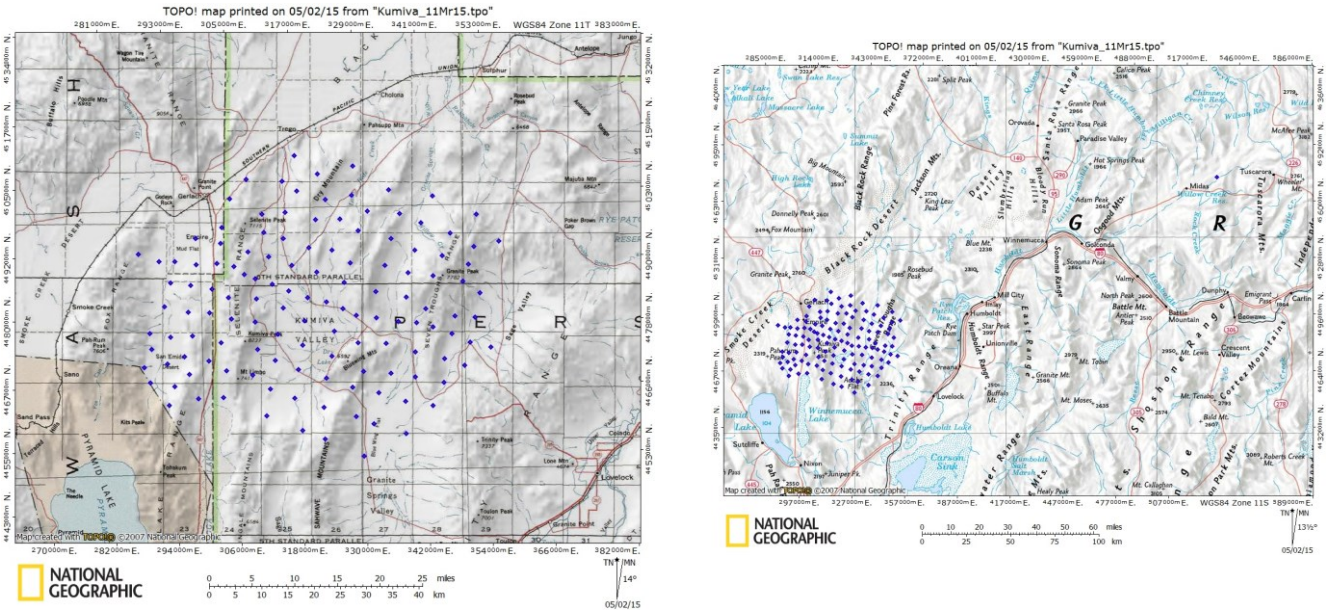

Figure 11: Left (a), Detailed site map for the MT surveying over the Kumiva Valley region, northwestern Nevada. There are a total of 131 stations. Right (b), Larger scale site map for Kumiva MT surveying showing location of the remote reference east of the village of Midas, NV.

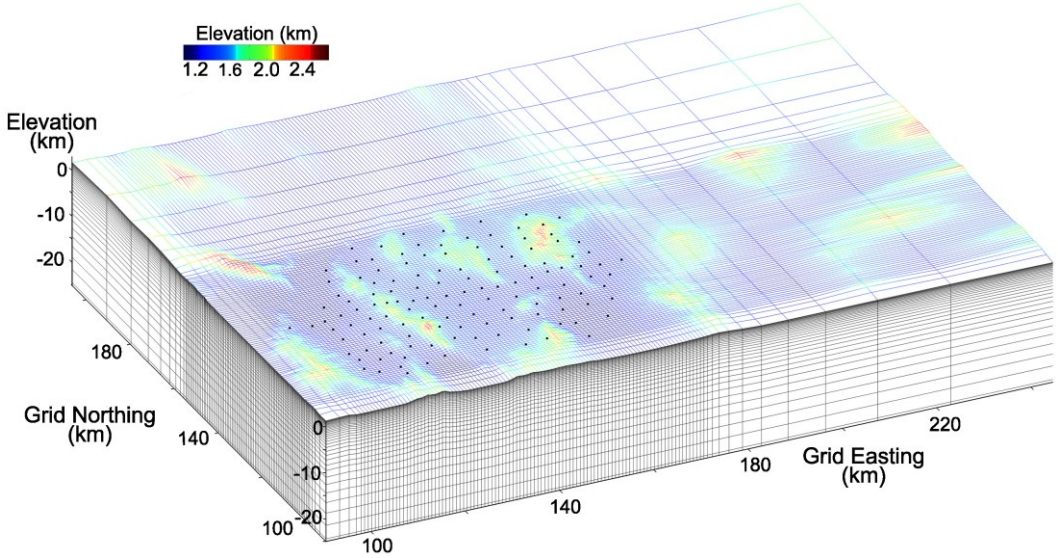

Figure 12: Central portion of hexahedral edge finite element mesh used in the 3D inversion of the Kumiva Valley and surroundings MT data set. Inversion was performed using the DOE/GTO-funded algorithm of Kordy et al. (2016a,b).

High quality MT results were obtained and formatted for 3D inversion using the edge finite element algorithm recently developed by our group under DOE/GTP support and described in Kordy et al. (2016a,b) (Figure 11). The finite element mesh was of dimension 104x by 127y by 62z cells giving nearly 600,000 parameters, with those in the middle of the mesh being 750-1000 m on a side and those near the surface being 85 m thick (Figure 12). Topography was defined using the NASA SRTM resource (Farr and Kobrick, 2000). There were 28 frequencies from 50 to 0.0047 Hz included utilizing all 12 elements of the complex MT response with error floors of 0.05|(Zxy-Zyx)/2| for impedance and 0.04 for tipper. Convergence to a normalized root-mean-square (nRMS) value of 1.31 from a starting value of 19.5 was obtained monotonically in 12 iterations on a 24-core server-class workstation with 0.5 TB RAM.

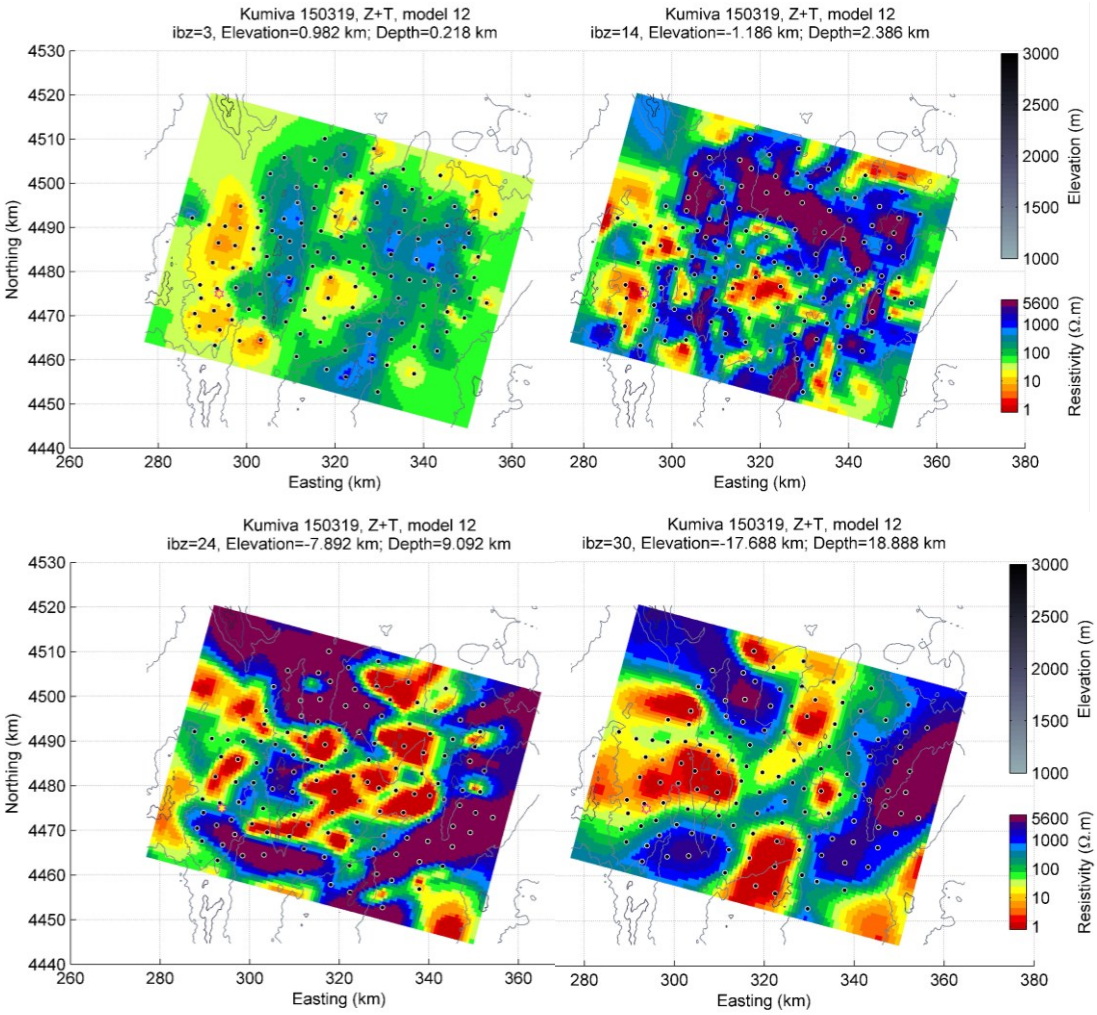

Figure 13: Four plan view slices through 3D MT inversion model of the Selenite Range-Kumiva Valley-Seven Troughs Range area. San Emidio geothermal prospect plotted as open star in southwest portion of project area. Depth label denotes average depth below surface of the deformed element layer whose resistivity is plotted. Elevation is the average elevation of that deformed layer.

Plan views through the 3D MT model are presented in Figure 13 with section views in Figure 14. The 3D results generally confirm the 2D results (Wannamaker et al., 2007; Siler et al., 2014; Dobson, 2016) but with greater detail and off-transect context. Local low resistivity upwellings are seen toward west flank of Seven Troughs Range and west of the Blue Wing Mountains (Kumiva Valley Playa). There also is such an upwelling under the San Emidio geothermal system dipping steeply to the north. A localized low resistivity anomaly also lies directly east of Blue Wing Flat in northern Granite Springs Valley. The resistivity features constitute the primary target areas for followup structural geology assessment and soil gas geochemistry discussed next.

4.2 Geological Mapping and Analysis

Because the region generally lacked detailed fault mapping, Coauthor Faulds and structural coworkers included all known Quaternary faults from the 2006 USGS data base and in some areas modified this database as a layer in analysis for potential blind systems. Initially, this work focused on identification and reconnaissance of favorable structural settings in the area. Subsequently, detailed geologic mapping and structural analysis focused on the aforementioned low resistivity anomaly in the vicinity of the central part of the Seven Troughs Range, which corresponded to a particularly favorable hybrid (fault intersection and step-over) structural setting (e.g., Faulds et al., 2013; Forson, 2014; Forson et al., 2014, 2015) (Figure 15). Geologic reconnaissance and preliminary structural analysis was also carried out over the low-resistivity anomaly within Kumiva Valley playa west of the Blue Wing Mountains (Figure 13), where a diffuse accommodation zone was identified, but the faults in this area appeared to be relatively inactive. Independently, we also investigated structurally the Black Warrior geothermal system just outside the southwest corner of the study area as a possible example similar to potential blind geothermal systems in other parts of the Kumiva study area (Sadowski and Faulds, 2015).

Subsequent to this initial work, much of the Kumiva Desert region has been incorporated into the Nevada play fairway analysis project (Faulds et al., 2016a,b), investigating additional structurally favorable regions as depicted in Figure 15. Parameters incorporated into the permeability modeling for the play fairway project included: 1) age of Quaternary faults, 2) slip rates on Quaternary faults, 3) horizontal

gravity gradient, 4) geodetic strain rate, 5) slip and dilation tendency, and 6) frequency of earthquakes. Comprehensive statistical analyses (e.g., weights of evidence) were used to estimate the relative weights of all internal items comprising each parameter, between each parameter (e.g. gravity vs. strain rate), and between permeability groups. The local, intermediate, and regional permeability were then synthesized into "combined permeability", which was incorporated with temperature at 3 km depth to produce a geothermal potential or play fairway map. Additional narrowing criteria were imposed, including available geophysical data, recency of faulting, presence of paleo-geothermal features, and availability of well data (Faulds et al., 2018). With these criteria applied, Granite Springs Valley was selected for detailed analysis.

Of several favorable settings within Granite Springs Valley, we found that northern Granite Springs Valley had the greatest potential. Integration of geologic, geochemical, and geophysical data was therefore undertaken for the area directly east of Adobe Flat in northern Granite Springs Valley. This area contains newly discovered sinter, silicified sands, and tufa deposits. It also corresponds to a low MT resistivity anomaly at the southeast edge of the array, and warm temperature-gradient wells are nearby (Figures 16 and 17). This site appears to occupy the southern termination of a major west-dipping normal fault that bounds the Seven Troughs Range on the west farther to the north. The sinter is confined to an ~1 km2 area.

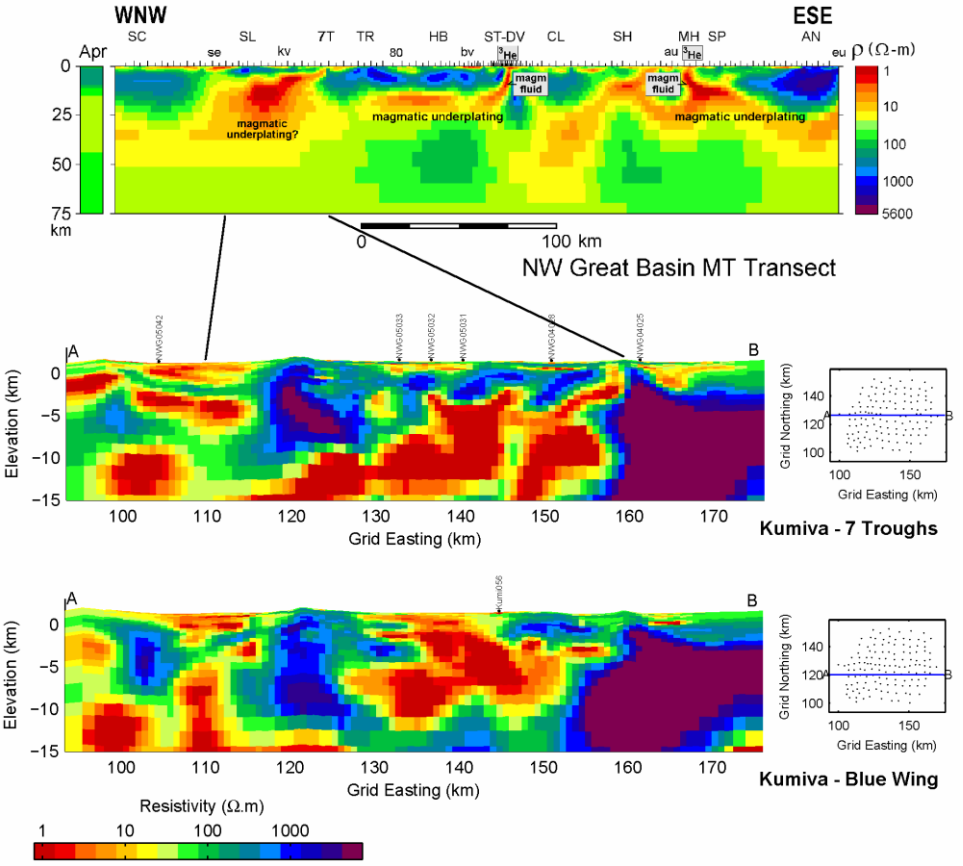

Figure 14: 2D and 3D section view slices through the San Emidio-Kumiva Valley-Seven Troughs Range area. Central Kumiva – Seven Troughs (7T) 3D section corresponds to western portion of 2D section at top, where 2D low resistivity upwelling under 7T symbol is that in the 3D section at km 158. Lower Kumiva – Blue Wing 3D section passes through low resistivity upwelling under Kumiva Valley (kv) Playa displayed in plan view in Figure 12 for depth of 2.4 km.

4.3 Soil Gas Geochemistry

Three soil gas surveys including isotope sampling in the final survey were carried out in the September – October time frame in 2015-2017. The cumulative results of soil gas study are summarized below. Based largely on the foregoing MT and structural data and analysis, Kennedy, Wannamaker and Faulds identified several areas of interest in Kumiva Valley (AOIs A - H, Figure 18) that were addressed by soil gas surveys. In general, CO_2 fluxes were low (~0.5 gm/m^2/day). Only three study areas significantly exceeded this background: G, A and D. The most promising flux anomaly was identified in AOI G (Figure 19b), a transect through a dilation zone near Seven Troughs Range Pass where earlier exploratory surveys identified a thermal anomaly (T ~ 14.7-17 ºC at 2 m) using a 2 meter probe (Forson et al., 2014a,b). Within the thermal anomaly, CO_2 fluxes as high as ~5 gm/m^2/day were observed and spatially correlated with a mapped fault trace and a historic mine entrance. A prominent MT upwelling occurs under the western flank of the range also.

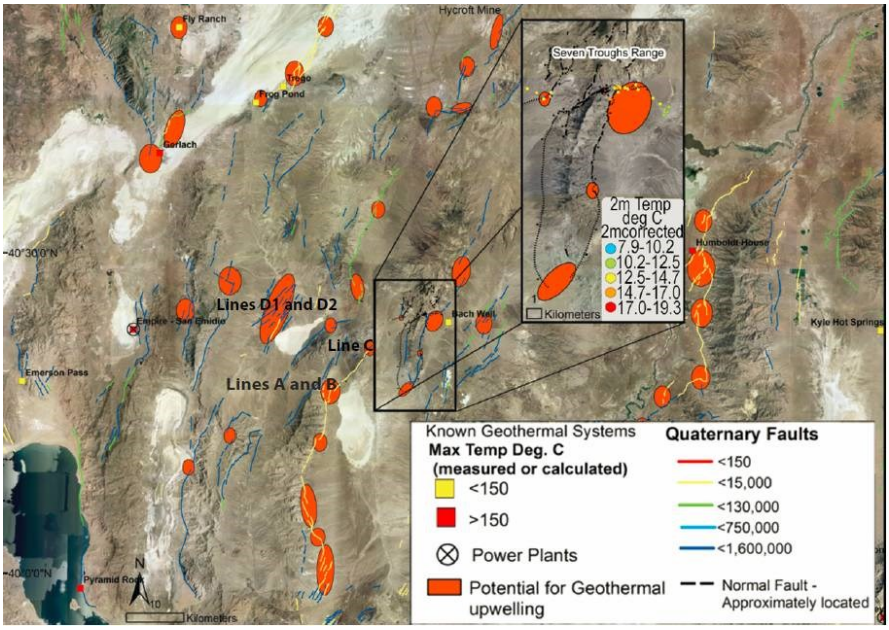

Figure 15: Possible areas of geothermal potential in the area surrounding the Kumiva Valley MT transect anomaly (from Forson, 2014a,b). Faults are from the USGS database (2006). Orange ellipses represent areas with favorable structural settings. The inset shows the Seven Troughs Range, a region where 2 m temperature surveying suggested occurence of warm ground.

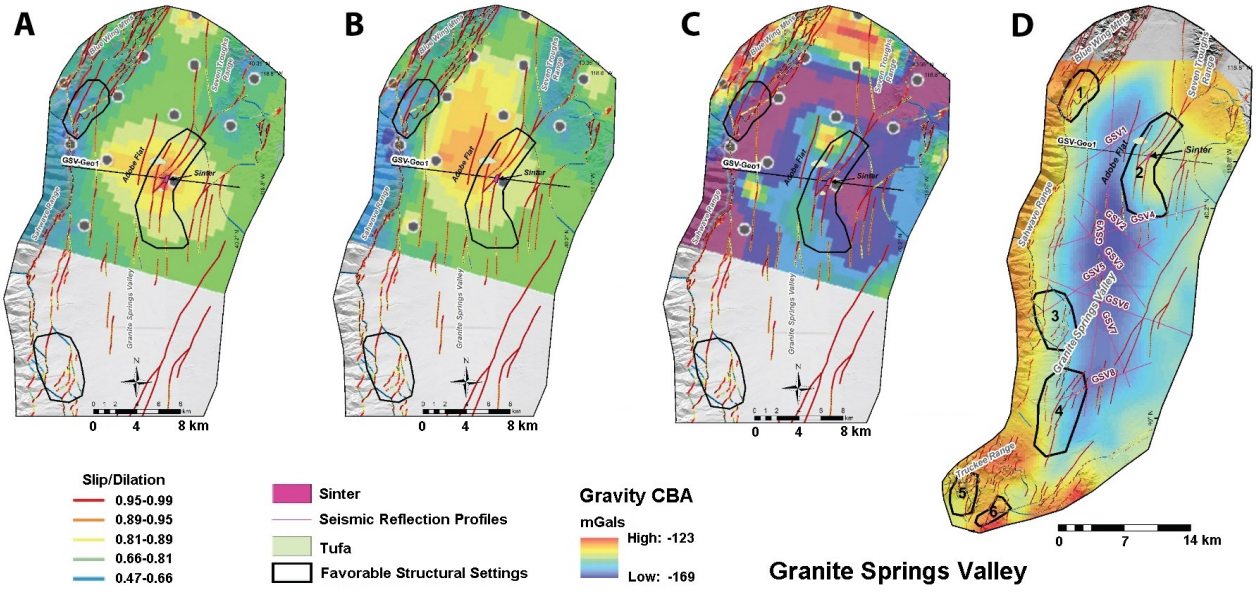

Figure 16: Granite Springs Valley area. Favorable structural settings are outlined in black, with setting #2 in northern Granite Springs Valley the highest priority in this area. A. Slip and dilation tendency and MT data slice at 0.127 km; note the low resistivity co-located with the sinter deposit. B. Slip and dilation tendency with a low resistivity anomaly at 0.565 km. C. Low-resistivity anomaly at 4.77 km. D. Complete Bouguer gravity anomaly. Cross section GSV-Geo1 shown in Figure 17.

A reproducible flux anomaly crossing a fault scarp in area A was also identified in the east-west pass separating the Granite Springs Mountains to the south from the Blue Wing Mountains to the north (Figure 19). At this time, it is not clear if this anomaly is associated with the fault or related to a shift in vegetation. South of Site A, a second anomaly occurs while crossing the fault scarp which runs along the eastern edge of the Granite Springs (Sahwave) Range, the same fault scarp surveyed at Site A (not plotted).

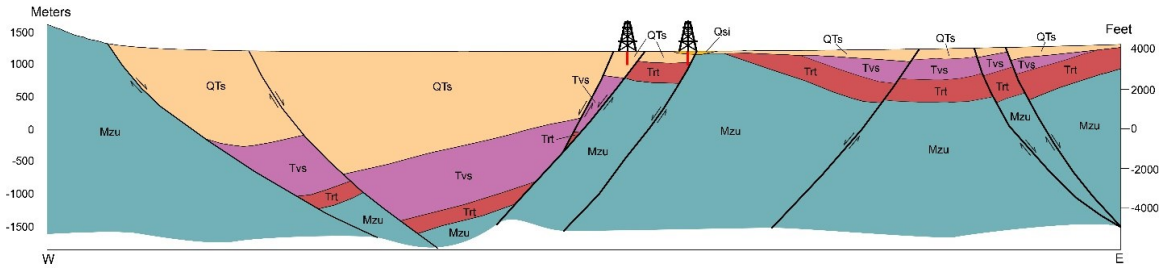

Figure 17: E-W cross section in northern Granite Springs Valley through Adobe Flat area, showing W-tilted half graben of the Granite Springs basin and W-dipping normal fault zone on the east side of basin that controls recent hydrothermal activity (sinter deposition). See Figure 16 for location (GSV-Geo-1). Proposed drilling sites for the play fairway project are shown. Qsi: silica sinter; QTs: late Miocene to Quaternary basin-fill sediments; Tvs: Miocene volcanic and sedimentary rocks; Trt: Oligocene ash-flow tuffs; Mzu: Mesozoic granitic and metamorphic rocks.

Three profiles were acquired across the Quaternary faults from the USGS data base marked west of the Blue Wing Mountains along the west flank of a large playa, denoted here as Kumiva Valley Playa (Area D). Toward the southern end of the fault distribution and playa, a modest CO_2 flux anomaly is observed that is rather distributed areally (line D2, Figure 20a). Profiling further north remained near background. No elevated CO_2 was observed along the short transect H in northeast Granite Springs Valley near the newly mapped sinter noted above.

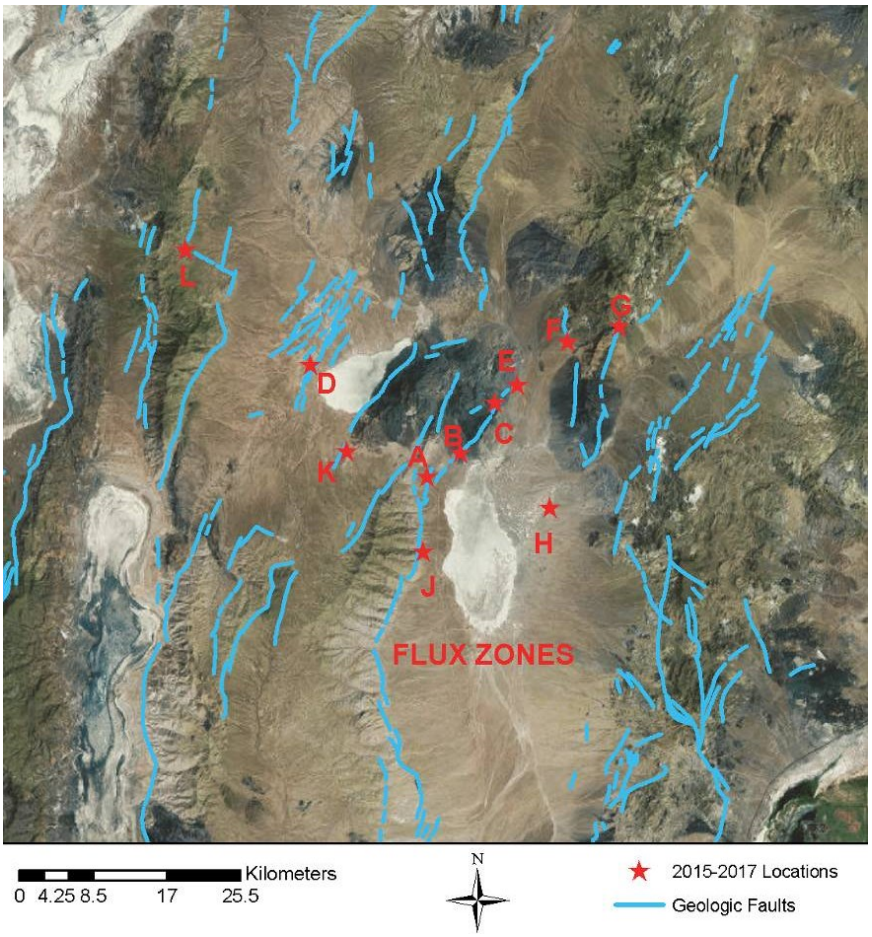

Figure 18: Study areas of interest (AOIs) for soil gas collection over the project area.

Soil gas was collected at ~0.5-1.0 meter depths using a pipette probe in AOIs A and G for carbon isotope analysis in the 2017 survey. The ^{13}C isotope content is plotted against flux value in Figure 20b. One sees a positive correlation between overall flux magnitude and ^{13}C concentration in the gas. One source of excess ^{13}C is from thermal breakdown of deep carbonate rocks or from magmatic sources. Although inferential, because ^{13}C concentration is correlated with vigor of soil degassing, its presence is suggestive of deep thermal processes connected through fault zone permeability to shallower levels. Similar to our study at McGinness Hills also, soil gas samples were sent to the Center for Accelerator Mass Spectrometry at Lawrence Livermore National Lab for ^{14}C analyses. Recall that if the samples consistently are depleted in ^{14}C relative to modern day carbon, then the source must have a deeper (non-surficial) abiotic origin. However, the ^{14}C results showed values that were within 98% of atmospheric (not plotted) and did not bear significant deep abiotic component. Thus, the soil gas indicators in the Kumiva-Black Rock study area are less diagnostic than at the McGinness Hills system. Potentially this is consistent with the more diffuse upwelling MT low-resistivity structures compared to McGinness Hills or Dixie Valley.

There being no current geothermal development in this greenfield area, there are no production fluid intervals to sample for ^{3}He occurrence. Porter Spring, nearby to the west of the Seven Troughs Range, has devolved into a swamp with spring feeds obscure and containing substantial human trash.

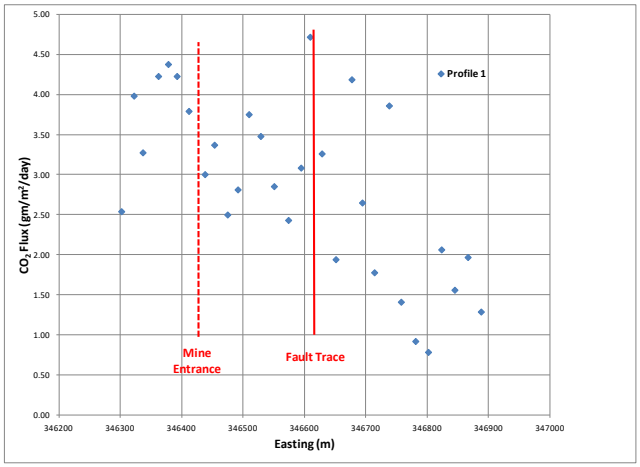

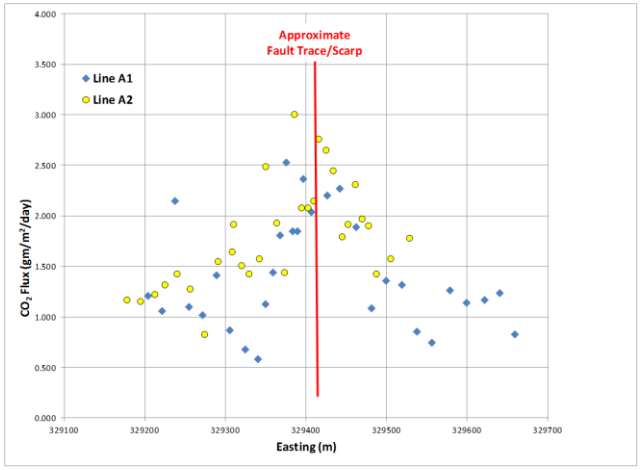

Figure 19: Left (a): CO_2 flux along profile near Seven Troughs Range pass in AOI G (Figure 18). Note the generally elevated flux and the spatial correlation with mapped fault traces. Right (b): CO_2 flux along Profiles A1 and A2 of AOI A.

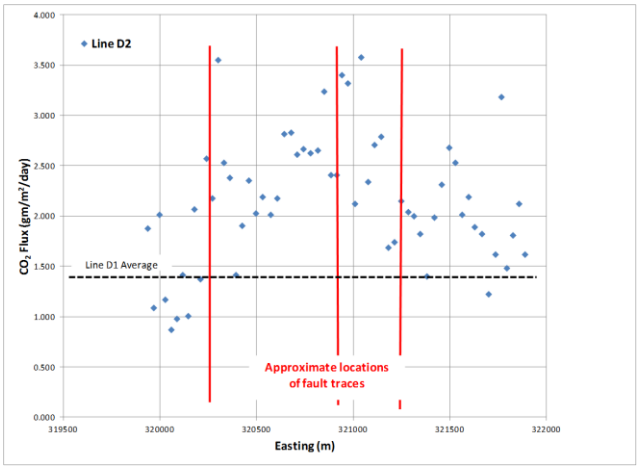

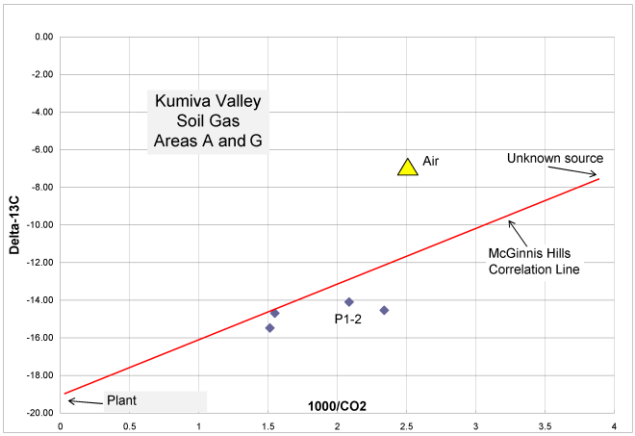

Figure 20: Left (a): CO_2 flux along Profile D2 along southwestern margin of Kumiva Valley playa on the west side of the Blue Wing Mountains (AOI D) (Figure 18). Del-^{13}C vs CO_2 flux in AOI G near Seven Troughs Range pass and area A in northwestern Granite Springs Valley. Sample P1-2 is from near Seven Troughs mine entrance. Right (b). The Del-13C correlation line for McGinness Hills is in red. None of these samples showed significant non-surficial ^{14}C content.

4.4 Conclusions of Kumiva Valley Study

The comprehensive 3D MT survey and inversion for the Kumiva Valley study area revealed several promising low-resistivity upwelling structures which showed reasonable agreement with the earlier 2D MT transect model in the area of overlap. The structural geology component of the project successfully identified numerous zones of potential dilatancy that were field-checked and subjected to detailed mapping in chosen focus areas. Several structural areas could be correlated with MT low-resistivity upwelling structures and targeted for soil gas transects. Three substantial field campaigns for CO_2 soil gas flux revealed generally low fluxes, but areas with flux do seem to correlate with promising structures and the most prominent low-resistivity upwellings. This is a large project area and further geochemical sampling would likely uncover more or further refine areas of interest. Given no current geothermal development in this greenfield area, there are no production fluid intervals to sample for ^{3}He occurrence. The favorable zone in northern Granite Springs Valley is receiving further attention in the University of Nevada Reno play fairway analysis project (Faulds et al., 2019).

5. GENERAL CONCLUSIONS

This project examined two geothermal areas, one now well into development and the other with potential, to determine whether certain geoscientific indicators were diagnostic of resource. These indicators are steeply-dipping, low-resistivity, presumed fluidized fault zones connecting to deep crustal magmatism, dilatant 3D geological structures that create space and pathways for geothermal reservoir fluids, and fluid and gas compositions including their isotopes that reflect deep-seated high-temperature sources. The Phase I study of the McGinness Hills system was clearly positive in this regard. It possesses one of the most pronounced MT structures of this character, was shown to have elevated ^{3}He as well as elevated ^{13}C and ^{14}C content in the production fluids, and lies in a well-developed structural accommodation zone between master Quaternary normal faults of opposing dip. The strongly positive indicators at McGinness Hills are in keeping with its proven generation capacity, recently being expanded to 134 MWe (Elko Daily Free Press, March 15, 2018) making it the largest geothermal power plant in Nevada.

The results of the greenfield Kumiva-Black Rock study area in Phase II are also viewed as positive although this district is more complex than McGinness Hills. Several prominent low-resistivity upwellings were identified from the 3D MT survey, but none show the sharpness of focus toward the surface of those seen with Dixie Valley or McGinness Hills. Moreover, soil gas flux anomaly A does not show a clear deep-seated MT anomaly, although admittedly this area is at the SE tip of the MT array coverage. However, it is unlikely to be the only exploitable occurrence in the Kumiva Valley district and more focused looks at the western Blue Wing Mountains or Seven Troughs Range Pass areas may be fruitful. The process could be improved somewhat if techniques were developed to assess ^{3}He fluxes to the surface that did not require active spring of producing well fluids to provide samples (see Dame et al., 2015). In many regards, our efforts here have constituted a proto-play fairway analysis through defining a geothermal exploration model and prioritizing followup investigation through multi-criteria decision making processes (Wannamaker et al., 2017; Faulds et al., 2019).

ACKNOWLEDGEMENTS

This project was generously funded by U.S. Department of Energy/Geothermal Technologies Office contract DE-EE005514 to the University of Utah. Development of the 3D finite element inversion algorithm of Kordy et al (2016a,b) was supported by DOE/GTO contract DE-EE002750 to the University of Utah. Partial funding was also provided by DE-EE0006731, the Nevada play fairway analysis project awarded to the University of Nevada, Reno. Quantec Geoscience Inc collected the MT data over the McGinness Hills and Kumiva Valley areas. The CO_2 concentrations, del^{13}C isotopic measurements and the He isotope measurements were all made at the Center for Isotope Geochemistry, Lawrence Berkeley National Laboratory. The ^{14}C analyses were conducted at the Center for Accelerator Mass Spectrometry (CAMS), Lawrence Livermore National Laboratory. Very kind assistance by Ormat personnel Ben Delwiche and Lara Owens enabled production and fluid sampling, and expanded our understanding of the structural picture. We are thankful for the cooperation of the U.S. Bureau of Land Management (Battle Mountain Office) and U.S. Forest Service (Ely Office) in permitting the MT surveying.

REFERENCES

Amundson R., Stern L., Baisden T., and Wang Y., 1998, The isotopic composition of soil and soil-respired CO_2: Geoderma, 82, 83-114.

Casaceli, R. J., D. E. Wendell, and W. D. Hoisington, 1986, Geology and mineralization of the McGinness Hills, Lander County, Nevada: in, Tingley, J. V., and H. F. Bonham, Jr., eds., Precious metal mineralization in hot springs systems, Nevada-California, Nevada Bureau of Mines and Geology, Report 41, 93-102.

Catchings, R. D., and W. D. Mooney, 1991, Basin and Range crustal and upper mantle structure, northwest to central Nevada: J. Geophys. Res., 96, 6247-6267.

Cerling T. E., D. K. Solomon, J. Quade, and J. R. Bowman 1991, On the isotopic composition of carbon in soil carbon dioxide: Geochim. Cosmochim. Acta 55, 3403-3405.

Coolbaugh, M. F., G. B. Arehart, J. E. Faulds, and L. J. Garside, 2005, Geothermal systems in the Great Basin, western United States: Modern analogues to the roles of magmatism, structure, and regional tectonics in the formation of gold deposits: Geological Society of Nevada Symposium, 1063-1082.

Crossey, L. J., and K. E. Karlstrom, 2012, Travertines and travertine springs in eastern Grand Canyon: wha they tell us about groundwater, paleoclimate and incision of Grand Canyon: Geological Society of America, Special Paper, 489, 131-143.

Dame, B. E., D. K. Solomon, W. C. Evans, and S. E. Ingebritsen, 2015, Developing a new, passive diffusion sampler suite to detect helium anomalies associated with volcanic unrest: Bulletin of Volcanology, 77, 17 pp.

Dobson, P., 2016, A review of exploration methods for discovering hidden geothermal systems: Geothermal Resources Council Transactions, 40, 695-706.

Farr, T. G., and M. Kobrick, 2000, Shuttle radar topography mission produces a wealth of data: EOS, Transactions AGU, 81, 583–585.

Faulds, J. E., and N. H. Hinz, 2015, Favorable tectonic and structural settings of geothermal systems in the Great Basin region, western USA: proxies for discovering blind geothermal systems: Proceedings World Geothermal Congress, Melbourne, 19-25 April, 4 pp.

Faulds, J. E., C. D. Henry, M. F. Coolbaugh, L. J. Garside, and S. B. Castor, 2005, Late Cenozoic Strain Field and Tectonic Setting of the Northwestern Great Basin, Western USA: Implications for Geothermal Activity and Mineralization: Geological Society of Nevada Symposium, 1091-1104.

Faulds, J. E., N. H. Hinz, M. F. Coolbaugh, P. H. Cashman, C. Kratt, G. Dering, J. Edwards, B. Mayhew, and H. McLachlan, 2011, Assessment of favorable structural settings of geothermal systems in the Great Basin, U.S.A.: Geothermal Resources Council Transactions, 35, 777-783.

Faulds, J. E., N. H. Hinz, G. M. Dering, and D. L. Siler, 2013, The hybrid model – the most accommodating structural setting for geothermal power generation in the Great Basin, western USA: Geothermal Resources Council Transactions, 37, 4-10.

Faulds, J. E., N. H. Hinz, M. F. Coolbaugh, L. A. Shevenell, and D. L. Siler 2016a, The Nevada play fairway project — Phase II: Initial search for new viable geothermal systems in the Great Basin region, western USA: Geothermal Resources Council Transactions, v. 40, p. 535-540.

Faulds, J.E., N. H. Hinz, M. F. Coolbaugh, D. L. Siler, L. A. Shevenell, J. H. Queen, C. M. dePolo, W. C. Hammond, and C. Kreemer, 2016b, Discovering geothermal systems in the Great Basin region: an integrated geologic, geochemical, and geophysical approach for establishing geothermal play fairways: Proceedings, 41st Workshop on Geothermal Reservoir Engineering, Stanford University, Stanford, CA, 15 pp.

Faulds, J.E., J. W. Craig, M. F. Coolbaugh, N. H. Hinz, J. M. Glen, S. Deoreo, 2018, Searching for blind geothermal systems utilizing play fairway analysis, western Nevada: Geothermal Resources Council Bulletin, 47, 34-42.

Faulds, J. E., N. H. Hinz, M. F. Coolbaugh, A. R. Ramelli, J. M. Glen, D. L. Siler, B. Ayling, and P. E. Wannamaker, 2019, Vectoring into potential blind geothermal systems in Granite Springs Valley, western Nevada: Application of the Play Fairway Analysis at multiple scales: paper presented at 43rd Workshop on Geothermal Reservoir Engr, Stanford, CA, SGP-TR-214.

Forson, C., 2014, Prospecting for a blind geothermal system utilizing geologic and geophysical data, Seven Troughs Range, northwestern Nevada [M.S. thesis]: University of Nevada, Reno, 87 pp.

Forson, C., J. E. Faulds, and P. E. Wannamaker, 2014, Prospecting for a blind geothermal system utilizing geologic and geophysical data, Seven Troughs Range, northwestern Nevada: Geothermal Resources Council Transactions, 38, 369-376.

Forson, C., J. E. Faulds, and M. D. Allen, 2015, Preliminary geologic map of the southern and central Seven Troughs Range, potential geothermal area, Pershing County, Nevada: Nevada Bureau of Mines and Geology Open-File Report 15-6, 6 pp.

Hickman, S.H., and N.C. Davatzes, 2010, In-Situ Stress and Fracture Characterization for Planning of an EGS Stimulation in the Desert Peak Geothermal Field, Nevada: Proceedings 35th Workshop on Geothermal Reservoir Engineering, Stanford University, Stanford, California, February 1-3.

Kennedy, B. M., and M. C. van Soest, 2006, A helium isotope perspective on the Dixie Valley, Nevada, hydrothermal system: Geothermics, 35, 26-43.

Kennedy, B. M., and M. C. van Soest, 2007, Flow of mantle fluids through the ductile lower crust: helium isotope trends: Science, 318, 1433-1436.

Kordy, M. A., P. E. Wannamaker, V. Maris, E. Cherkaev, and G. J. Hill, 2016a, Three-dimensional magnetotelluric inversion using deformed hexahedral edge finite elements and direct solvers parallelized on SMP computers, Part I: forward problem and parameter jacobians: Geophysical Journal International, 204, 74-93.

Kordy, M. A., P. E. Wannamaker, V. Maris, E. Cherkaev, and G. J. Hill, 2016b, Three-dimensional magnetotelluric inversion using deformed hexahedral edge finite elements and direct solvers parallelized on SMP computers, Part II: direct data-space inverse solution: Geophysical Journal International, 204, 94-110.

Maris, V., and P. E. Wannamaker, 2010, Parallelizing a 3D finite difference MT inversion algorithm on a multicore PC using OpenMP: Computers & Geosciences, doi: 10.1016/j.cageo.2010.03.001, 5 pp.

Nordquist, J., and B. Delwiche, 2013, The McGinness Hills geothermal project: Geothermal Resources Council Transactions, 37, 57-63.

Rhodes, G. T., 2011, Structural control on the Empire-San Emidio Desert geothermal system, northwestern Nevada: [M.S. thesis], University of Nevada, Reno, 72 pp.

Rhodes, G. T., J. E. Faulds, and W. Teplow, 2010, Structural controls of the San Emidio Desert geothermal field, northwestern Nevada: Geothermal Resources Council Transactions, 34, 819-822.

Sadowski, A., and J. Faulds, 2015, The structural controls of the Black Warrior blind geothermal system, Truckee Range, Washoe-Churchill counties: Geothermal Resources Council Transactions, 39, 573-580.

Sadowski, A. J., and J. E. Faulds, 2016, Preliminary geologic map of the Black Warrior geothermal area, Truckee Range, Washoe and Churchill Counties, Nevada: Nevada Bureau of Mines and Geology Open-File Report 16-7, scale 1:24,000, 6 pp.

Sasaki, Y., 2004, Three-dimensional inversion of static-shifted magnetotelluric data: Earth, Planets and Space, 56, 239-248.

Siler, D. L., and J. E. Faulds, 2013, Three-dimensional geometry fairway mapping: Examples from the western Great Basin, USA: Geothermal Resources Council Transactions, 37, 327-332.

Siler, D.L., and B. M. Kennedy, 2016, Regional crustal-scale structures as conduits for deep geothermal upflow: Geothermics, 59, 27–37. https://doi.org/10.1016/j.geothermics.2015.10.007, 11pp.

Siler, D. L., B. M. Kennedy, P. E. Wannamaker, 2014, Regional lithospheric discontinuities as guides for geothermal exploration: Geothermal Resources Council Transactions, 38, 39-47.

Sorey, M., et al., 1998, Carbon dioxide and helium emissions from a reservoir of magmatic gas beneath Mammoth Mountain, California: J. Geophys. Res., 103(B7), 15,303-15,315.

Tarantola, A., 1987, Inverse problem theory, Elsevier, New York, 671 pp.

Wannamaker, P., P. Rose, W. Doerner, B. Berard, J. McCulloch, and K. Nurse, 2004, Magnetotelluric surveying and monitoring at the Coso geothermal area, California, in support of the Enhanced Geothermal Systems concept: survey parameters, initial results: Proceedings 29th Workshop on Geothermal Reservoir Engineering, Stanford, CA, SGP-TR-175, 8 pp.

Wannamaker, P. E., W. M. Doerner, and D. P. Hasterok, 2006a, Cryptic faulting and multi-scale geothermal fluid connections in the Dixie Valley-Central Nevada Seismic Belt area; implications from MT resistivity surveying: Proceedings 31st Workshop on Geothermal Reservoir Engineering, Stanford University, Stanford, CA.

Wannamaker, P. E., D. P. Hasterok, and W. M. Doerner, 2006b, Possible magmatic input to the Dixie Valley geothermal field, and implications for district-scale resource exploration, inferred from magnetotelluric (MT) resistivity surveying: Geothermal Resources Council Transactions, 30, 471-475.

Wannamaker, P. E., W. M. Doerner, and D. P. Hasterok, 2007, Integrated dense array and transect MT surveying at Dixie Valley geothermal area, Nevada; structural controls, hydrothermal alteration and deep fluid sources: Proceedings 32nd Workshop on Geothermal Reservoir Engineering, Stanford, CA, SGP-TR-183, 6 pp.

Wannamaker, P. E., D. P. Hasterok, J. M. Johnston, J. A. Stodt, D. B. Hall, T. L. Sodergren, L. Pellerin, V. Maris, W. M. Doerner, and M. J. Unsworth, 2008, Lithospheric dismemberment and magmatic processes of the Great Basin-Colorado Plateau transition, Utah, implied from magnetotellurics: Geochemistry, Geophysics, Geosystems, 9, Q05019, doi:10.1029/ 2007GC001886, 36 pp.

Wannamaker, P. E., V. Maris, D. Hasterok, and W. Doerner, 2011, Crustal Scale Resistivity Structure, Magmatic-hydrothermal connections, and thermal regionalization of the Great Basin: Geothermal Resources Council Transactions, 35, 1787-1790.

Wannamaker, P., V. Maris, J. Sainsbury, and J. Iovenitti, 2013, Intersecting fault trends and crustal-scale fluid pathways below the Dixie Valley geothermal area, Nevada, inferred from 3D magnetotelluric surveying, Proceedings 38th Workshop on Geothermal Reservoir Engineering, Stanford, CA, SGP-TR-198, 6 pp.

Wannamaker. P. E., J. N. Moore, K. L. Pankow, S. F. Simmons, G. D. Nash, V. Maris, A. Trow, and C. L. Hardwick, 2017, Phase II of Play Fairway Analysis for the Eastern Great Basin extensional regime, Utah: status of indications: Geothermal Resources Council Transactions, 41, 2368-2382.